Molecular Therapy
Nucleic Acids
Original Article

Glutamine missense suppressor transfer RNAs inhibit polyglutamine aggregation

Rasangi Tennakoon,[1] Teija M.I. Bily,[1] Farah Hasan,[1] Sunidhi Syal,[1] Aaron Voigt,[2] Tugce B. Balci,[3] Kyle S. Hoffman,[4] and Patrick O'Donoghue[1,5]

[1]Department of Biochemistry, The University of Western Ontario, London, ON N6A 5C1, Canada; [2]Department of Neurology, RWTH Aachen, 52062 Aachen, Germany; [3]Department of Paediatrics, The University of Western Ontario, London, ON N6A 5C1, Canada; [4]Bioinformatic Solutions, Inc, Waterloo, ON N2L 3K8, Canada; [5]Department of Chemistry, The University of Western Ontario, London, ON N6A 5C1, Canada

Huntington's disease (HD) is caused by polyglutamine (polyQ) repeat expansions in the huntingtin gene. HD-causative polyQ alleles lead to protein aggregation, which is a prerequisite for disease. Translation fidelity modifies protein aggregation, and several studies suggest that mutating one or two glutamine (Gln) residues in polyQ reduces aggregation. Thus, we hypothesized that missense suppression of Gln codons with other amino acids will reduce polyQ aggregate formation in cells. In neuroblastoma cells, we assessed tRNA variants that misread Gln codons with serine ($tRNA^{Ser}_{C/UUG}$) or alanine ($tRNA^{Ala}_{C/UUG}$). The tRNAs with the CUG anticodon were more effective at suppressing the CAG repeats in polyQ, and serine and alanine mis-incorporation had differential impacts on polyQ. The expression of $tRNA^{Ser}_{CUG}$ reduced polyQ protein production as well as both soluble and insoluble aggregate formation. In contrast, cells expressing $tRNA^{Ala}_{CUG}$ selectively decreased insoluble polyQ aggregate formation by 2-fold. Mass spectrometry confirmed Ala mis-incorporation at an average level of ~20% per Gln codon. Cells expressing the missense suppressor tRNAs showed no cytotoxic effects and no defects in growth or global protein synthesis levels. Our findings demonstrate that tRNA-dependent missense suppression of Gln codons is well tolerated in mammalian cells and significantly reduces polyQ levels and aggregates that cause HD.

INTRODUCTION

Huntington's disease (HD) is one of nine hereditary neurodegenerative diseases caused by an expansion of CAG (glutamine, Q) trinucleotide repeats.[1] Exon 1 of the Huntingtin gene (HTTexon1) normally encodes a polyglutamine (polyQ) tract ranging from 10 to 35 CAG codons, while mutant HTT (mHTTexon1) generates an expanded HTT protein with >35Q.[2] Longer polyQ stretches encoded by uninterrupted CAG repeats are associated with an earlier age of onset and increase in disease severity; however, the relationship between polyQ length and health outcomes is variable.[3,4]

The HTT protein is most abundant in striatal neurons and glial cells.[5] Although the cellular function of full-length HTT is not entirely understood, in neurons, HTT is associated with vesicle transport, axonal trafficking, and apoptotic signaling.[6] HTT-containing polyQ tracts in the pathological range exhibit a propensity to aggregate into high-molecular-weight protein complexes enriched in β sheet structures.[7] Normal cellular proteins may become tangled in the aggregates, and their presence initiates further disruption of protein homeostasis.[8] Neuronal degeneration in HD typically begins in neurons of the basal ganglia, resulting in motor, cognitive, and psychiatric symptoms that worsen over time due to the progressive nature of HD.[9] There is currently no cure or treatment for HD beyond those that attempt to relieve the symptoms. Antisense oligonucleotides (ASOs) are nucleic-acid-based therapeutic approaches to HD that aim to reduce polyQ-containing protein production and aggregation.[10] IONIS-HTT_{RX} is a non-selective total HTT-lowering ASO that recently progressed to phase 3 clinical trials. The ASO reduced mutant HTT protein levels by 20%–42% in the central nervous system, with no serious adverse effects observed in patients. Although this trial was discontinued after a patient risk/benefit assessment,[10,11] the same ASO (tominersen) is now in phase 2 trials (ClinicalTrials.gov: NCT05686551) to assess dosage levels and target patients with early-stage HD. In addition, several silencing RNA therapies are advancing through phase 1/2 clinical trials,[12] and these approaches have shown reductions in wild-type and mutant polyQ levels to 20% of those found in untreated HD mice.[13]

Studies on amino acid interruptions in polyQ and the development of peptide inhibitors to disrupt and reduce polyQ aggregation[14] point toward potential HD therapies. Biophysical studies showed that amino acid substitutions in polyQ can reduce aggregation, while work in mammalian cells found that proline (Pro) interruptions in polyQ blocked aggregate formation.[15,16] In another polyQ disease, spinocerebellar ataxia type 1 (SCA1), interruptions with two histidine (His) residues led to significant delays in the age of onset for patients and reduced aggregation kinetics in cells.[17] Fascinatingly, in the context of reduced transfer RNA $(tRNA)^{Gln}_{CUG}$ levels, cells produce

Received 21 June 2024; accepted 19 December 2024;
https://doi.org/10.1016/j.omtn.2024.102442.

Correspondence: Patrick O'Donoghue, Department of Biochemistry, The University of Western Ontario, London, ON N6A 5C1, Canada
E-mail: patrick.odonoghue@uwo.ca

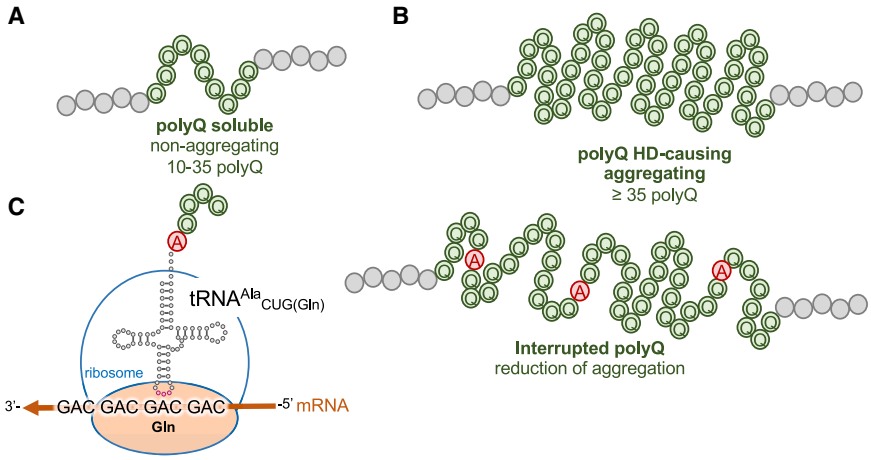

Figure 1. Mechanisms of polyQ aggregation and tRNA-dependent missense suppression of huntingtin

(A) Wild-type huntingtin less than 35 glutamine repeats does not aggregate. (B) Mutant huntingtin with an expanded polyQ tract leads to protein aggregation and disease. (C) Anticodon mutations in $tRNA^{Ala}$ cause mis-incorporation of alanine at glutamine sites in polyQ tracts.

a higher level of +1 *trans*-frame species from the CAG repeat, which contains poly-Ser peptides that modulate aggregation.[18,19] Knockdown of the tRNA modification enzyme TRMT2A in human embryonic kidney (HEK)293T cells caused a reduction of 103Q aggregation, and the polyQ aggregates were less toxic than in cells with normal TRMT2A levels.[20] Elevated levels of glutamate mis-incorporation at Gln codons were detected in TRMT2A-knockdown cells using a luciferase missense reporter assay, and insoluble polyQ aggregates were reduced in flies with TRMT2A silenced.[21] Together, these studies reaffirm that reducing polyQ aggregation is an important goal for HD therapeutics[22,23] and that mistranslation of glutamine codons may reduce polyQ protein aggregation.

Translation fidelity relies on the accurate ligation of each tRNA with its cognate amino acid. The aminoacyl-tRNA synthetases (aaRSs)[24] select their cognate tRNA by recognizing nucleotide identity elements in the tRNA structure.[25,26] The anticodon sequence in the tRNA anticodon loop is commonly an identity element, yet many tRNAs require additional or sometimes distinct identity elements for recognition.[25,26] For example, seryl-tRNA synthetase (SerRS), leucyl-tRNA synthetase (LeuRS), and alanyl-tRNA synthetase (AlaRS) do not recognize the anticodon.[25,26] The major identity element for AlaRS is the G3:U70 base pair in $tRNA^{Ala}$, while nucleotides in the acceptor stem, especially the discriminator base at position 73, and the long variable arms in serine ($tRNA^{Ser}$) and leucine ($tRNA^{Leu}$) tRNAs serve as major identity elements for their cognate aaRSs.[26] Thus, single-nucleotide substitutions in the anticodon of $tRNA^{Ser}$, $tRNA^{Leu}$, or $tRNA^{Ala}$ genes can result in mistranslation across the entire proteome in mammalian cells.[27–29]

Indeed, human genomes include both rare and surprisingly common human tRNA variants that cause mistranslation.[30] We have characterized natural variants found in $tRNA^{Ser}$,[27,31] $tRNA^{Ala}$,[28] $tRNA^{Gly}$,[28] and $tRNA^{Leu}$ [29] that all cause amino acid mis-incorporation when the tRNA is expressed in human or murine cells. Genetic interactions between naturally occurring human missense suppressor tRNAs and neurodegenerative alleles revealed the potential for tRNAs to impact protein aggregation. In one example, a $tRNA^{Ser}_{AGA}$ G35A ($tRNA^{Ser}_{AAA}$) variant that occurs in 2% of individuals[27] causes mis-incorporation of Ser at phenylalanine (Phe) codons in multiple mammalian cell lines, inhibits protein production, and exhibits synthetic toxicity with proteasome inhibition. In cells expressing the mutant $tRNA^{Ser}_{AAA}$ and HTTexon1 74Q, polyQ aggregates were slower to form compared to polyQ aggregates in cells expressing the wild-type $tRNA^{Ser}$.[27] In a model of amyotrophic lateral sclerosis (ALS), we found that the expression of $tRNA^{Ser}_{AAA}$ caused synthetic or super-additive toxicity with an ALS-causative allele but not with a wild-type variant of the fused in sarcoma (FUS) protein in mammalian cells.[31]

Synthetic missense suppressor tRNAs are an emerging therapeutic avenue that can ameliorate disease-causing mutations by incorporating a wild-type or tolerable amino acid at the mutation site.[32–35] Since anticodon variants of $tRNA^{Ala}$ and $tRNA^{Ser}$ are efficiently aminoacylated, they are ideal candidates for effective missense suppression. Indeed, a human $tRNA^{Ser}$ engineered to decode isoleucine (Ile) was able to suppress translation and inhibit tumor formation in xenograft mouse models.[36] Missense suppressors can also be used to rescue disease-causing missense mutations. In HEK293T cells, a $tRNA^{Arg}$ suppressor capable of misreading glutamine codons partially corrected a pathogenic Arg-to-Gln mutation in Ca^{2+}-activated cysteine protease calpain 3 (CAPN3) that causes limb-girdle muscular dystrophy type 2A.[33]

Together, these studies suggest that missense suppressor tRNAs and translational fidelity can impact protein production and protein aggregation that causes disease. To test our hypothesis that mis-incorporation of different amino acids in the polyQ tract of HTT will reduce aggregation, we designed four missense suppressor tRNAs that cause the mis-incorporation of serine or alanine at glutamine codons (Figures 1 and S1). We found that the expression of $tRNA^{Ser}_{CUG}$ reduced both 23Q and 74Q protein levels and eliminated nearly all polyQ aggregation in murine neuroblastoma cells. In contrast, cells expressing $tRNA^{Ala}_{CUG}$ reduced insoluble, but not soluble, polyQ aggregate formation in cells. The missense suppressor tRNAs caused no significant cytotoxic effects, changes in cell growth rate, or defects in global protein synthesis. Our findings demonstrate that glutamine missense suppressor tRNAs are well tolerated and inhibitory of HTT protein production and aggregation in cells.

Table 1. Human tRNA activity-level predictions for tRNA genes

	tRNAscan-SE score	Average phyloP score	CpG density	Probability of activity	Expression of ARM/CHIP
Average of active tRNAs	76.2	0.86	0.0430	92.1%	
tRNA-Ala-AGC-8-1	59.7	1.63	0.0595	97.2%	+/+
tRNA-Ser-AGA-2-3	89.6	0.649	0.0435	98.5%	+/+

Human tRNA gene activity predictions and gene properties are derived from Thornlow et al.[34] ARM, AlkB RNA methylation sequencing (ARM-seq) of tRNAs indicated expression (+)[38,41]; CHIP, chromatin immunoprecipitation sequencing (CHIP-seq) data also supported expression from the indicated genomic loci (+).[42,43]

RESULTS

Identifying tRNA genes used in this study

The aaRSs selective for $tRNA^{Ser}$ and $tRNA^{Ala}$ do not use the anticodon sequence as an identity element. Nonsynonymous anticodon mutations in $tRNA^{Ser}$ and $tRNA^{Ala}$ change codon recognition without affecting aminoacylation by the cognate aaRS. Thus, these anticodon variants incorporate Ser or Ala at codons intended for other amino acids, leading to mistranslated proteins.[27,28] We generated missense suppressor tRNAs to mis-incorporate Ser or Ala at Gln codons and determined their impact on polyQ protein production and aggregation. Based on our previous experience showing that the G35A variant of the tRNA-Ser-AGA-2-3 gene is an effective missense suppressor of Phe codons,[27] we created synthetic variants with CUG or UUG glutamine anticodons (Figure S1). Both anticodons are known to decode the CAG codon[37] like those in our polyQ constructs. Since the CUG anticodon is more efficient in CAG decoding, we anticipated that tRNAs with the CUG anticodon may have a greater impact on polyQ aggregation relative to missense suppressors with the UUG anticodon. By searching the genomic tRNA database,[34,38] tRNA-Ala-AGC-8-1 was selected to create missenses suppressors with glutamine anticodons (C/UUG) based on a confident prediction of constitutive activity (97.2%; Table 1; Figure S1) and documented expression of the tRNA in human cells.[38–40]

Production of polyQ proteins in normal and missense-suppressing cells

Given the need to easily quantify polyQ protein production and aggregation, we used GFP-tagged HTT alleles that are well-established models of HD.[27,44] We conducted experiments in murine Neuro2a (N2a) neuroblastoma cells due to their long-standing use as models of HD,[27,45,46] because they are easily transfected to high efficiency, and because they are a neuronal-like cell line similar to the native tissues where HD pathology occurs.

To assess the effect of glutamine missense suppressor tRNAs on polyQ protein production, wild-type (EGFP-23Q) or polyQ-expanded (EGFP-74Q) and fluorescently tagged HTT alleles were co-expressed in N2a cells from the same plasmid also expressing no additional tRNA, wild-type $tRNA^{Ser}_{AGA}$, or a $tRNA^{Ser}$ or $tRNA^{Ala}$ variant with UUG or CUG anticodons. We used fluorescence microscopy to observe EGFP-23Q and -74Q production in live cells. At 72 h after transfection, in comparison with cells expressing no tRNA, the expression of wild-type $tRNA^{Ser}$ leads to a minor but significant 1.2-fold increase in 74Q and no change in 23Q levels in cells. In contrast, in cells expressing the Gln-decoding $tRNA^{Ser}_{CUG}$, we observed significant decreases in EGFP-23Q (20-fold) and -74Q (2-fold) fluorescence per cell (Figures 2A and 2B) relative to cells expressing no additional tRNA. The reduction in fluorescence of EGFP-tagged 23Q and 74Q proteins in cells expressing $tRNA^{Ser}_{CUG}$ was confirmed to result from reduced protein levels by western blotting (Figures 3A and 3B). Cells expressing $tRNA^{Ser}_{UUG}$ showed a small but significant 1.1-fold increase in EGFP-74Q fluorescence per cell (Figures 2A and 2B), while cells expressing $tRNA^{Ala}_{CUG}$ showed minor 1.2-fold reductions of EGFP-23Q and -74Q fluorescence per cell (Figures 2A and 2B). The minor changes (1.1- to 1.3-fold) observed in the fluorescence microscopy were not sufficiently different to be discernably changed in the western blot, as no significant changes in EGFP-23Q or -73Q protein levels were seen in the western blot from cells expressing no additional tRNA or any of the wild-type or missense suppressor tRNAs (Figures 2C and 2D) except for $tRNA^{Ser}_{CUG}$.

To ensure that the impact on fluorescence is related to mis-incorporation in the polyQ tracts, we conducted a control experiment in N2a cells that were transfected with a GFP-mCherry fusion protein encoded on the same plasmid with no additional tRNA, wild-type $tRNA^{Ala}$, or $tRNA^{Ala}_{CUG}$. Relative to the condition with no additional tRNA, we observed a modest but significant increase in GFP and mCherry fluorescence per cell in cells expressing the mutant $tRNA^{Ala}$ and a greater increase in GFP and mCherry fluorescence in cells with wild-type $tRNA^{Ala}$ (Figure S2). Thus, the Gln-decoding $tRNA^{Ala}$ mutant does not diminish GFP fluorescence and even increases GFP production in a construct lacking the polyQ tract.

We[27–29] and others[47] have observed that missense suppressor tRNAs lead to different impacts on protein homeostasis that depend on the amino acid substitution and the anticodon sequence. Reduced protein production efficiency is a hallmark response to mistranslation in mammalian cells. Thus, we were not surprised to observe that $tRNA^{Ser}_{CUG}$ reduces the ability of transfected cells to produce the EGFP-polyQ constructs, while the other tRNA variants show more minimal perturbations to protein production. To confirm these effects on polyQ synthesis in a human cell model of HD, each tRNA suppressor was next expressed in human neuroblastoma (SH-SY5Y) cells. As in the N2a cells, EGFP fluorescence was reduced in 74Q cells expressing $tRNA^{Ser}_{CUG}$ (1.8-fold) and $tRNA^{Ala}_{CUG}$ (1.4-fold) (Figures 3A

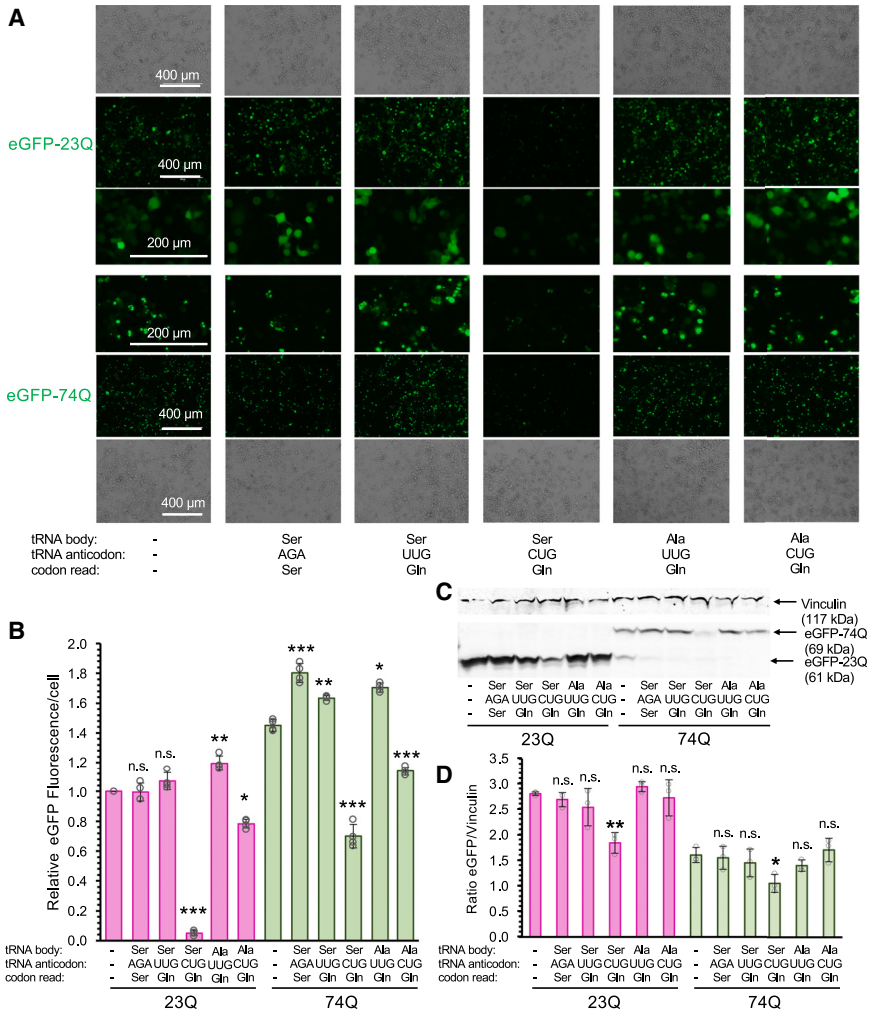

Figure 2. EGFP-polyQ protein levels in wild-type and mistranslating murine neuroblastoma (N2a) cells

(A) Bright-field and fluorescent images showing EGFP-polyQ production in cells co-expressing 23Q or 74Q and the indicated tRNA anticodon variants 72 h post-transfection. (B) Quantification of mean EGFP fluorescence per cell shows the level of GFP-23Q or -74Q production in individual cells. (C) Western blot and (D) quantation of the blot for EGFP with a vinculin loading control shows that the Gln-decoding $tRNA^{Ser}$ with the CUG anticodon reduces production of 23Q and 74Q, while other tRNA variants did not substantially affect total polyQ protein levels 72 h post-transfection. Error bars show ±1 standard deviation of the mean of $n = 4$ biological replicates. Asterisks indicate p values from independent sample t tests (n.s., no significant difference, $^{*}p < 0.05$, $^{**}p < 0.01$, and $^{***}p < 0.001$).

and 3B). However, in SH-SY5Y cells, the decrease in EGFP-23Q fluorescence in cells with $tRNA^{Ala}_{CUG}$ was greater (1.5-fold) than in N2a cells (Figures 3A and 3B). In contrast, the decrease of 1.6-fold in 23Q production caused by co-expression with $tRNA^{Ser}_{CUG}$ was less substantial in human relative to mouse cells.

To determine whether the $tRNA^{Ser}_{CUG}$ and $tRNA^{Ala}_{CUG}$ glutamine suppressors affect global protein synthesis, we used the surface sensing of translation (SUnSET) method[48] to measure protein synthesis levels in SH-SY5Y cells. The SUnSET assay utilizes the aminoacyl-tRNA analog puromycin, which is incorporated into nascent peptide chains, to quantify global protein levels in cells through the immunodetection of puromycin incorporated in the proteome.[48] Compared to a vinculin loading control, no changes were seen in puromycin levels in any of the tested cell lines. Global protein production levels were not significantly different in cells expressing 23Q, 74Q, or the Ala or Ser missense suppressors (Figure S3). Thus, the glutamine codon missense-suppressing tRNAs had greater impacts on EGFP-polyQ production than on global protein levels.

To determine if the tRNA mutants induce the integrated stress response, we next examined phosphorylation of eukaryotic initiation factor 2α (eIF2α) (Figure S4). Increased phosphorylated eIF2a (p-eIF2α) levels are a hallmark of proteotoxic stress and a signal that slows translation by inhibiting translation initiation.[49,50] Mistranslation, of a sufficient kind and level, can stimulate phosphorylation of eIF2α at Ser51.[47] We transfected SH-SY5Y cells with a plasmid bearing GFP-23Q and no additional tRNA or the $tRNA^{Ser}$ or $tRNA^{Ala}$ CUG anticodon variants. We observed no changes in eIF2α or p-eIF2α levels (Figure S4). We also confirmed the tRNAs caused no significant increase in the stoichiometry eIF2α phosphorylation (Figure S4E). The data suggest that the Gln-decoding $tRNA^{Ser}$ and $tRNA^{Ala}$ variants do not stimulate the integrated stress response branch of the unfolded protein response (UPR) pathway in human cells.

Missense suppression reduces polyQ aggregates in cells

To characterize the impact of Gln codon suppression with Ser or Ala on polyQ aggregate levels, we applied an automated thresholding approach established previously.[27,51] The algorithm counts the area and number of intensely bright foci that represent polyQ aggregates in each transfected cell. In this approach, the intensely bright foci (see the materials and methods) are clearly differentiated from diffusely localized GFP-polyQ protein (Figure S5). Images were acquired at 72 h after transfection of N2a cells with plasmids co-expressing the EGFP-HTTexon1-23Q or -74Q and $tRNA^{Ala}$ or $tRNA^{Ser}$ Gln suppressors or controls lacking additional tRNA or with wild-type tRNA. As expected, no aggregates were observed in cells expressing EGFP-23Q with any of the tRNAs. In cells expressing EGFP-74Q and no additional tRNA, $tRNA^{Ser}_{AGA}$, $tRNA^{Ser}_{UUG}$, and $tRNA^{Ala}_{UUG}$

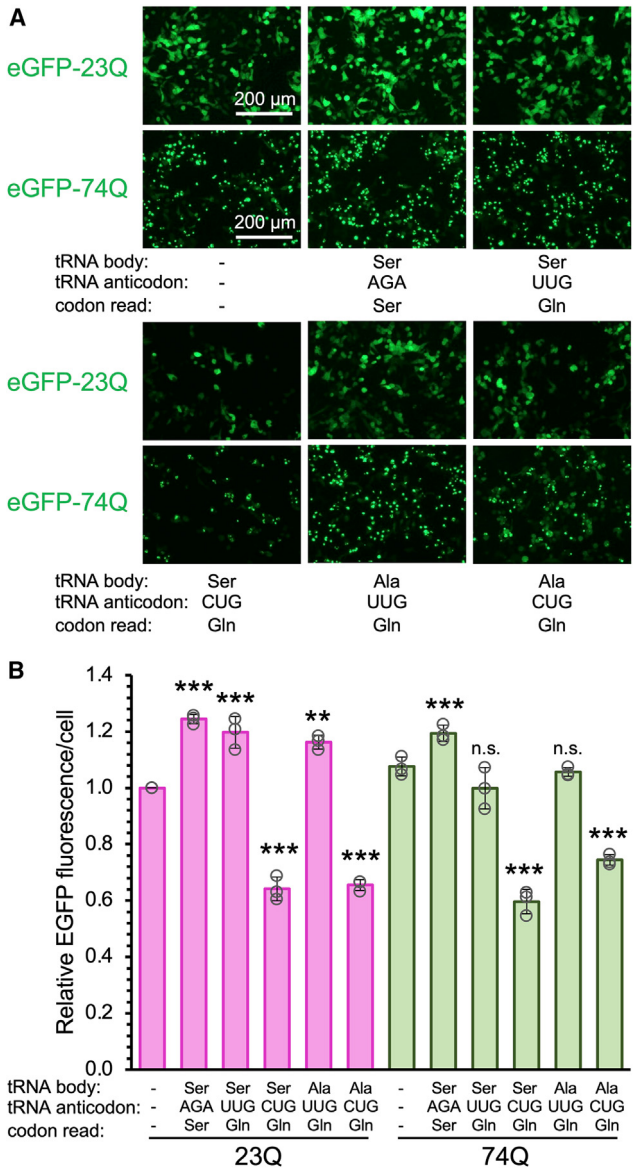

Figure 3. GFP-polyQ levels in human neuroblastoma cells

(A) Fluorescent images showing EGFP-polyQ production in cells co-expressing 23Q or 74Q and the indicated tRNA anticodon variants 72 h post-transfection in human SH-SY5Y cells. (B) Quantification of mean EGFP fluorescence per cell shows the level of GFP-23Q or -74Q production in individual cells. Error bars show ±1 standard deviation of the mean of $n = 4$ biological replicates. Asterisks indicate p values from independent sample t tests (n.s., no significant difference, $^{**}p < 0.01$, and $^{***}p < 0.001$).

all showed an average 0.60–0.70 aggregates per cell with no significant differences between their levels (Figure 4A). A ∼2-fold decrease to 0.36 aggregates per cell was observed in cells expressing Gln-decoding $tRNA^{Ala}_{CUG}$ compared to cells expressing 74Q and no additional tRNA (Figure 4A). While $tRNA^{Ser}_{CUG}$ reduced 74Q protein levels by 2-fold (Figures 2C and 2D), the mis-incorporation of Ser had an even greater impact on aggregate levels. Indeed, in N2a cells expressing $tRNA^{Ser}_{CUG}$ and 74Q (Figure 2), there were no bright foci above the background fluorescence level. Thus, $tRNA^{Ser}_{CUG}$ both reduces 74Q levels and nearly eliminates aggregation, while $tRNA^{Ala}_{CUG}$ acts more selectively to reduce 74Q aggregation.

To assess the missense suppressors in a homologous human cellular context, we also observed the number of aggregates formed in human SH-SY5Y cells co-expressing the tRNA controls or missense suppressors and EGFP-23Q or -74Q over a 72 h time course. Between 24 and 48 h, we observed a significant increase in the number of 74Q aggregates per cell in cells expressing $tRNA^{Ser}_{AGA}$, $tRNA^{Ser}_{UUG}$, and $tRNA^{Ala}_{UUG}$, which increased from 0.1 to 0.2 to ∼1.1 aggregates per cell (Figure 5). Interestingly, cells expressing 74Q and no additional tRNA did not develop as many aggregates until after 48 h and then reached 1.1 aggregates per cell at 72 h (Figures 4B and 5). In contrast, cells expressing 74Q and $tRNA^{Ser}_{CUG}$ or $tRNA^{Ala}_{CUG}$ showed significantly reduced levels of polyQ aggregates at 48 h (0.2 aggregates per cell) that remained suppressed at 72 h (0.4 aggregates per cell) (Figure 5A). Cells expressing the Ala or Ser tRNAs with the CUG anticodon showed significantly slower rates of aggregate formation compared to any other condition (Figure 5B). Thus, both Ser and Ala missense suppressors with the CUG anticodon inhibited 74Q aggregate formation in human and murine neuroblastoma cells.

PolyQ aggregation produces a range of different kinds of soluble oligomers and insoluble aggregates. We used a membrane detergent assay to measure the levels of insoluble polyQ aggregates in each cell line expressing EGFP-74Q. We imaged N2a cells at 72 h after transfection, before and immediately following treatment with Triton X-100. After the addition of the detergent, the soluble polyQ proteins and aggregates diffuse into the media and are no longer visible,[52] while the remaining fluorescent foci represent large and insoluble polyQ aggregates. To measure the fraction of insoluble polyQ aggregates and the number of insoluble aggregates remaining in cells following detergent treatment, we applied a thresholding analysis[27] to identify and quantify aggregates in each transfected cell. Cells expressing the non-aggregating EGFP-23Q following Triton X-100 treatment showed no fluorescence or evidence of insoluble aggregate formation as anticipated (Figure 6). While 74Q readily forms insoluble aggregates, cells expressing $tRNA^{Ser}_{CUG}$ did not form any insoluble 74Q aggregates (Figure 6).

By comparing the ratio of fluorescence after to before detergent treatment, we quantified the fraction of insoluble polyQ aggregates in each cell line (Figure 6B). We observed no significant changes in insoluble aggregate levels in cells expressing no additional tRNA, wild-type tRNA, or missense suppressors with the UUG anticodons. In these cells, insoluble aggregates account for 95%–98% of the total fluorescence observed in the cells prior to detergent treatment. We observed a significant 2-fold reduction in insoluble polyQ aggregates in cells expressing $tRNA^{Ala}_{CUG}$ and a nearly total elimination of insoluble aggregates in cells expressing $tRNA^{Ser}_{CUG}$. We then characterize the

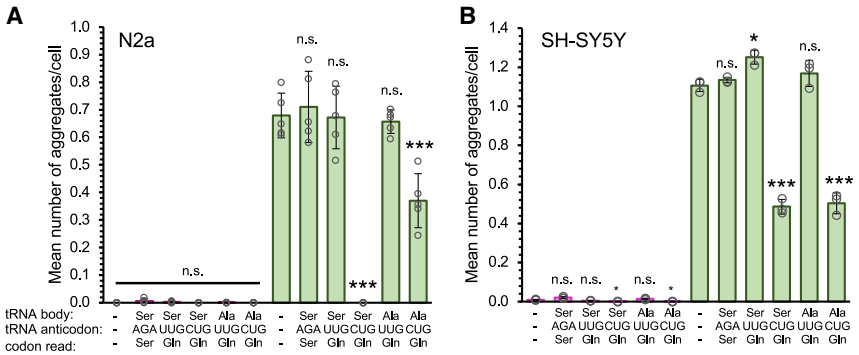

Figure 4. EGFP-polyQ aggregate levels in wild-type and missense-suppressing neuroblastoma cells

The average number of fluorescent polyQ aggregates per cell is plotted at 72 h post-transfection of (A) murine N2a and (B) human SH-SY5Y cells with plasmids bearing GFP-23 or -74Q and no tRNA (–) or the indicated $tRNA^{Ser}$ or $tRNA^{Ala}$ anticodon mutant. Aggregates are identified as intensely bright foci, defined as 18 standard deviations above the mean fluorescent pixel value, and quantitated using an automated image processing algorithm, as described before.[27] Error bars show ±1 standard deviation of the mean of (A) $n = 5$ or (B) $n = 3$ biological replicates. Asterisks indicate p values from independent sample t tests (n.s., no significant difference, $^{*}p < 0.05$, $^{**}p < 0.01$, and $^{***}p < 0.001$).

mean number of insoluble aggregates per cell remaining after detergent treatment (Figure 6C). We observed significant reductions in the number of insoluble aggregates visible after detergent treatment in cells expressing $tRNA^{Ser}_{UUG}$ (70%), $tRNA^{Ser}_{CUG}$ (0%), $tRNA^{Ala}_{UUG}$ (77%), and $tRNA^{Ala}_{CUG}$ (55%) compared to the aggregates observed in cells without additional tRNA or with wild-type tRNA. Thus, the tRNA missense suppressors can reduce both the fraction of insoluble polyQ protein and the number of insoluble polyQ aggregates in cells.

In the context of N2a cells expressing either 23Q or 74Q, the Gln-decoding missense suppressors showed no significant cytotoxic effects (Figure S6). We previously found that expression of 46Q or 74Q alone is not cytotoxic in N2a cells,[27] and this finding is in agreement with observations from others showing that HTT alleles up to 150Q are not toxic to N2a cells.[53] We had also found that co-expression of 46Q with $tRNA^{Ser}$ that decodes Phe codons was not cytotoxic; however, 46Q promoted synthetic or super-additive toxicity in cells expressing a tRNA that mis-incorporates Ser at proline (Pro) codons.[27] Thus, the level and kind of mis-incorporation generated by our Gln missense suppressors was not sufficient to induce toxicity with polyQ aggregates in N2a cells. We also measured proliferation over a 72 h time course in SH-SY5Y cells and found that none of the polyQ or tRNA variants impacted cell viability (Figure S7A) or the rate of cell growth (Figure S7B). The data suggest that that levels of Ser and Ala mis-incorporation at Gln codons are well tolerated under the conditions tested.

Estimating soluble polyQ aggregate levels

Although most of the 74Q aggregates are insoluble (Figure 6), we also characterized the impact of each tRNA variant on soluble polyQ aggregate levels using semi-denaturing detergent agarose gel electrophoresis (SDD-AGE). SDD-AGE is a semi-quantitative method used to visualize protein aggregates from soluble protein lysates as high-molecular-weight products, represented by smears above a defined band that is the monomeric or non-aggregating protein fraction. In the cells expressing 23Q, there are no significant levels of high-molecular-weight products as expected (Figure S8A). We again observed significantly less polyQ protein produced by cells expressing $tRNA^{Ser}_{CUG}$, in agreement with fluorescence microscopy (Figure 2) and western blotting (Figure 3). We observed that the 74Q protein made in cells expressing $tRNA^{Ser}_{CUG}$ migrated further in the gel, perhaps due to a higher Ser content. To estimate the level of high-molecular-weight soluble aggregates, we used densitometry to quantify the intensity of the 74Q smear (Figure S8B) as well as the level of the 74Q high-molecular-weight products relative to the level of the 74Q monomer band (Figure S8C). Similar to our observations with insoluble aggregates using microscopy (Figure 6), cells

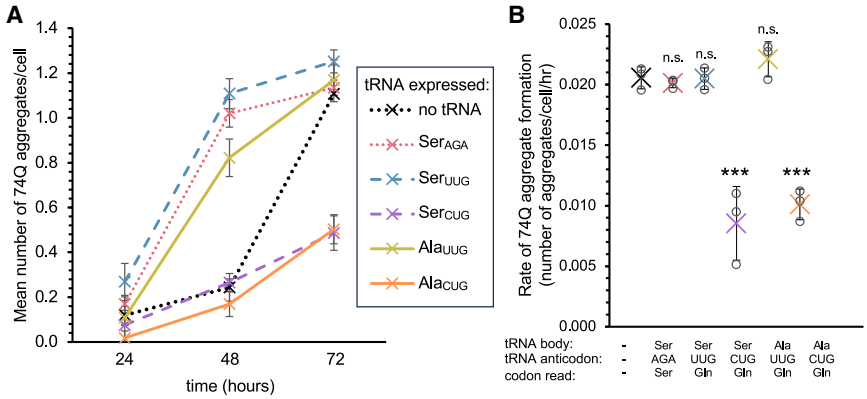

Figure 5. Rate of polyQ aggregate formation in human neuroblastoma cells

(A) Mean number of 74Q aggregates per cell in transfected SH-SY5Y cells at 24 h intervals and (B) the rate of 74Q aggregate formation (mean number of aggregates per cell per hour) over 72 h was calculated from the slope of each curve in (A). Error bars show ±1 standard deviation of the mean of $n = 3$ biological replicates. Asterisks indicate p values from independent sample t tests (n.s., no significant difference and $^{***}p < 0.001$).

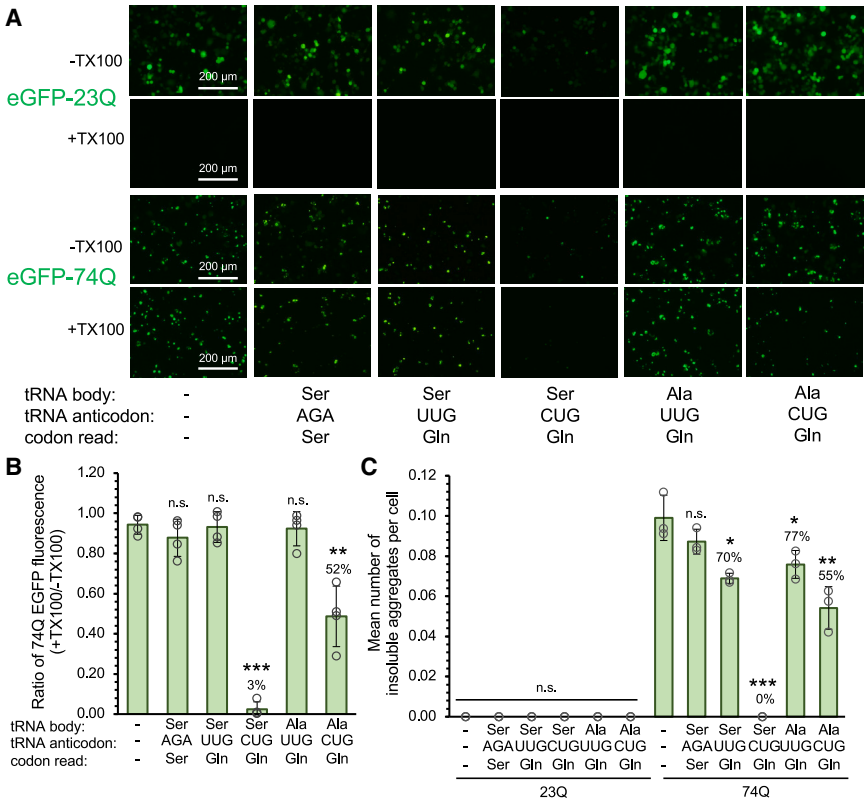

Figure 6. Suppression of insoluble 74Q aggregation in neuroblastoma cells

N2a cells were (A) imaged 72 h after transfection with a plasmid bearing wild-type (23Q) or deleterious (74Q) huntingtin alleles and no additional tRNA, wild-type $tRNA^{Ser}_{AGA}$, or the Gln-decoding $tRNA^{Ser}$ or $tRNA^{Ala}$ before and after Triton X-100 (TX100) treatment. (B) To estimate the fraction of total aggregates that are insoluble, we plotted the ratio of EGFP-74Q fluorescence from insoluble aggregates (+TX100) compared to the fluorescence prior to detergent treatment (−TX100). (C) The mean number of insoluble aggregates per cell remaining following detergent treatment was plotted. Error bars show ±1 standard deviation of the mean of at least $n = 3$ biological replicates. Asterisks indicate p values from independent sample t tests (n.s., no significant difference, $^{*}p < 0.05$, $^{**}p < 0.01$, and $^{***}p < 0.001$).

expressing $tRNA^{Ser}_{CUG}$ and $tRNA^{Ser}_{UUG}$ displayed lower overall levels of soluble polyQ aggregates (Figure S8B). In contrast, the $tRNA^{Ala}_{CUG}$ did not affect soluble polyQ aggregate levels (Figure S8B). We found a significant change in soluble aggregate relative to 74Q monomer levels only in cells expressing $tRNA^{Ser}_{UUG}$ that showed a reduced fraction of soluble aggregates (Figure S8C). Interestingly, there was no significant change in the level of soluble 74Q aggregates relative to monomeric 74Q protein in cells expressing $tRNA^{Ser}_{CUG}$ or $tRNA^{Ala}_{CUG}$ (Figure S8C). Together with our observations above, the data suggest that $tRNA^{Ala}_{CUG}$ exclusively disrupts insoluble, but not soluble, polyQ aggregates. In contrast, mis-incorporation with Ser shows the potential to modify both soluble and insoluble polyQ aggregation.

$tRNA^{Ala}_{CUG}$ mis-incorporates alanine into polyQ

We used liquid chromatography-tandem mass spectrometry (LC-MS/MS) to validate tRNA-dependent mis-incorporation of Ala in the polyQ tract produced in cells expressing EGFP-23Q (Figures 7 and S9; Tables 2 and S1). EGFP-23Q was isolated from N2a cells expressing $tRNA^{Ala}_{CUG}$ as well as from cells expressing no additional tRNA as a control. In cells expressing no additional tRNA, we identified no peptides that corresponded to Ala mis-incorporation in the polyQ tract (Figure 7A). We found one peptide that suggests Ala at two adjacent Gln residues in the EGFP portion of the molecule (Figure S9B), which is at low abundance (Figures 7C and 7D). In contrast, MS/MS analysis of immunoprecipitated GFP-23Q purified from cells expressing the missense suppressor tRNA identified multiple peptides corresponding to Ala mis-incorporation at nearly all of the Gln codons (17/23) in the polyQ tract (Figure 7; Table 2) as well as in Gln codons in the EGFP portion of the molecule (Figures 7 and S9A; Table S1). To highlight sites with relatively abundant mis-incorporation, Gln sites with Ala mis-incorporation of >2% ion intensity were annotated on the peptide coverage maps (Figures 7 and S9).

We then used the area under the monoisotopic peaks of the mis-incorporated peptides compared to the area under the peak for the matching properly translated peptides to estimate the level of mistranslation observed by MS at each Gln codon. In cells expressing EGFP-23Q and $tRNA^{Ala}_{CUG}$, we observed Ala mis-incorporation levels of 10%–20% on average (Figure 6C). We found that the fraction of mistranslated peptides in the polyQ tract compared to the EGFP segment of the construct was not significantly different. The data also show that the level of Ala mis-incorporation in the EGFP-23Q construct is significantly greater in cells expressing $tRNA^{Ala}_{CUG}$ compared to cells expressing no additional tRNA (Figures 7C and 7D). We attempted to analyze the EGFP-74Q protein in a similar fashion; however, due to the aggregating nature of this protein, coverage was low, and we were not able to identify peptides covering the polyQ tract. We successfully identify peptides representing about half of the EGFP portion of the EGFP-74Q molecule, including 2 sites and 3 independent peptide hits, confirming Ala mis-incorporation at Gln codons in the EGFP-74Q protein (Figure S10).

DISCUSSION

PolyQ protein synthesis in mistranslating cells

Our data show that missense suppressor tRNAs affect polyQ aggregation and production to different extents, depending on the cell type, the

Table 2. Summary of peptides identified by tandem mass spectrometry showing Gln and Ala incorporation at Gln codons in the polyQ portion of the EGFP-23Q protein

PolyQ residue	Maximal $-10\log_{10}(p)$	Ion counts, Ala (A)/Gln (Q)
Q258	61.55	6/78
Q259	60.41	3/81
Q260	73.94	4/80
Q261	65.77	6/76
Q262	82.46	6/72
Q263	80.66	7/67
Q264	62.49	3/66
Q265	74.41	6/56
Q266	73.17	3/52
Q267	51.20	2/51
Q268	71.72	4/36
Q269	77.70	2/33
Q270	73.55	1/26
Q271	75.07	2/21
Q272	62.42	1/24
Q273	38.62	1/21
Q277	56.84	1/6
Q292[a]	91.14	1/7

[a]Gln residue downstream of the poly-23Q and within HTTexon1.

nature of the mis-incorporated amino acid, and the anticodon sequence of the suppressor tRNA. In mammalian cells, reduced protein production is a characteristic of tRNA-dependent mistranslation.[5,35,47] Studies in HEK293 cells showed that the expression of a variety of $tRNA^{Ser}$ anticodon variants reduced the level of a GFP reporter protein in cells to different degrees.[47] The Gln-decoding $tRNA^{Ser}$ led to a minor (~10%) decrease in GFP production, while missense suppressors of other codons, including histidine, aspartate, and isoleucine, caused reduced GFP production by >1.5-fold.[47] Here, we found that in both murine and human neuroblastoma cells, the Gln-decoding $tRNA^{Ser}_{CUG}$ significantly inhibited 23Q and 74Q production and reduced 74Q aggregation. This finding is consonant with our previous studies on the interaction of polyQ alleles with a natural human $tRNA^{Ser}_{AGA}$ G35A variant that decodes Phe codons with Ser.[31,38] Mistranslation generated by $tRNA^{Ser}_{AAA}$ slowed 74Q aggregation, but these cells reached the same level of 74Q aggregation at 72 h relative to a control cell line expressing wild-type tRNA.[27] In contrast, $tRNA^{Ser}_{CUG}$ and $tRNA^{Ala}_{CUG}$ were able to maintain suppression of polyQ aggregates over the entire 72 h time course. While the $tRNA^{Ser}_{UUG}$ and Gln-decoding $tRNA^{Ala}$ variants did not impact polyQ production in N2a cells, we did observe reduced levels of EGFP-23Q and 74Q in human neuroblastoma cells expressing $tRNA^{Ala}_{CUG}$. Fascinatingly, none of the Gln-decoding missense suppressors impacted puromycin incorporation (Figure S3), suggesting a limited impact on global protein synthesis levels and a relatively greater and more selective impact on polyQ protein production and aggregation.

Differential impacts of $tRNA^{Ala}_{CUG}$ in human as compared to mouse cells may relate to differences in the expression level of the tRNA in the specific genetic background. In future studies, beyond the scope of this work, we will use quantitative tRNA sequencing approaches, as before,[29] to determine the level of each suppressor tRNA in each cell line. Since our mutant tRNAs differ by only 1 or 2 bases from the host background, tRNA sequencing methods emerged as the definitive method to quantify tRNA variants. Outside of the internal A and B box promoter sequences in the tRNA gene body, upstream and downstream extragenic sequences contain important transcriptional regulatory elements.[54] Indeed, detailed studies revealed sequences in the region 18–66 bases upstream of the tRNA body that were critical for efficient expression and activity of a $tRNA^{Ser}$ nonsense suppressor in mammalian cells.[55] Sequences flanking the tRNA body are generally not well conserved, even among tRNA isodecoder groups.[54] Differences between the mouse and human tRNA gene sequences, both in the tRNA gene body and in the up- and downstream regions (Figure S11), may contribute to differential expression and maturation of the tRNAs through a mechanism that is dependent on the host expression system.

Missense tRNA suppressors differentially impact soluble and insoluble polyQ aggregation

HTT is a large protein of 3,144 amino acid residues and a mass of ~350 kDa. Aggregation of HTT is a prerequisite to disease and linked to HD pathology.[56] In mice expressing a 102Q allele, initial neuropathology of HD stems from axonal transport dysfunction and degeneration linked to aggregate formation.[57] Changes in the size and number of dendrites in the striatum and cortex were observed in HD mouse models,[58,59] and neutrophil aggregates large enough to disrupt dendritic transport were also observed in the same tissues.[60] In HTT-138Q flies, the reduction of aggregation increased the lifespan, and no occurrences of reduced aggregation without improved viability were identified, suggesting aggregates as the toxic species in this model.[61] Moreover, quantitative analysis of aggregation kinetics in neurons revealed a connection between the biophysics of polyQ aggregation and age of onset and disease progression.[62,63] Interestingly, mice expressing full-length HTT with 140Q crossed with mice with a polyQ deletion experienced reduced aggregation and enhanced lifespan and showed only a mild HD phenotype compared to uncrossed 140Q mice.[64]

In normal cells and disease pathology, numerous studies have demonstrated that proteolytic cleavage of full-length HTT yields several amino-terminal fragments, the smallest of which is exon 1 that contains the pathogenic polyQ stretch associated with HD.[65–68] Furthermore, the HTT mRNA transcript can be subject to aberrant splicing, leading to the translation of the disease-causing HTTexon1 protein in HD human fibroblasts and mouse models.[69] Indeed, the insertion of HTTexon1-116Q in the genome triggers a progressing HD phenotype in transgenic mice within just 3 weeks.[70] HTTexon1 constructs also readily recapitulate the HD polyQ aggregation phenotype.[71] Thus, our studies employed fluorescently

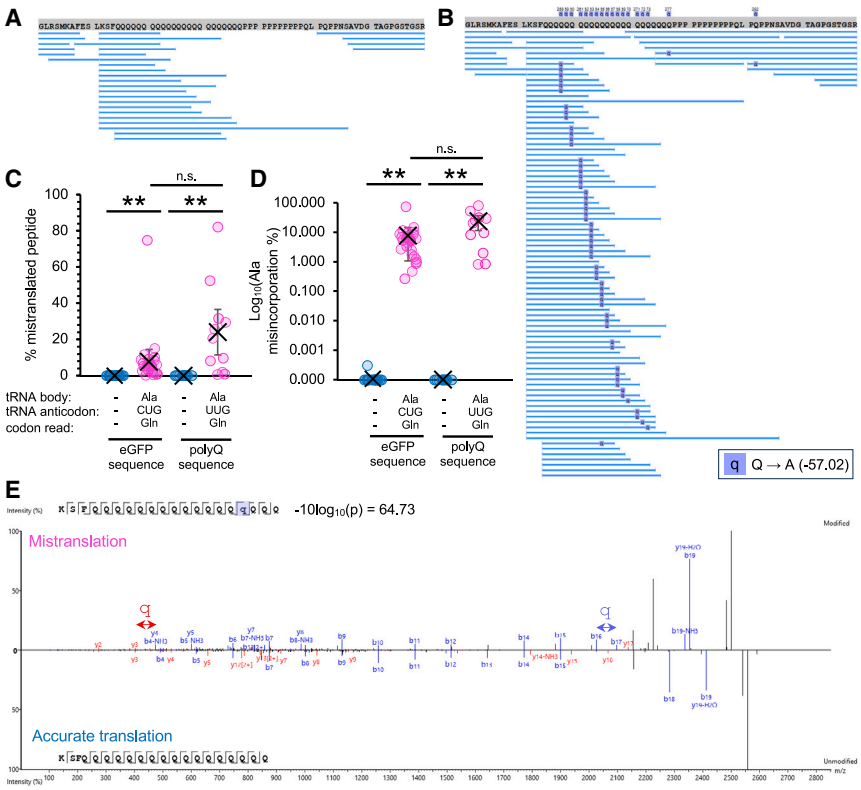

Figure 7. Tandem mass spectrometry reveals tRNA-dependent mis-incorporation of alanine in polyQ

Peptide coverage maps of tandem mass spectrometry analysis that were used to detect alanine mis-incorporation at glutamine sites in GFP-tagged HTTexon1-23Q isolated from N2a cells expressing (A) no additional tRNA or (B) $tRNA^{Ala}_{CUG}$ at 72 h post-transfection. (C) For all mistranslated peptides identified, the level of missense suppression was estimated by calculating the ratio of area under the isotopic peak for the mis-incorporated a peptide (mistranslation) relative to that of a corresponding wild-type peptide (accurate translation). (D) Logarithmic plot of the percentage of mistranslated peptides relative to properly translated peptides at glutamine codons in the EGFP sequence and the polyQ tract. (E) Example mirror y and b ion spectra comparing mistranslated (top) to a corresponding properly translated peptide (bottom). Lowercase q's in purple boxes indicate sites of alanine mis-incorporation at glutamine codons. Error bars show ±1 standard deviation of the mean of $n = 3$ biological replicates. Asterisks indicate p values from independent sample t tests (n.s., no significant difference and $^{**}p < 0.01$).

labeled polyQ alleles to enable the quantitation of HTT aggregates in live cells. We demonstrated that the co-expression of 74Q and missense suppressor $tRNA^{Ala}_{CUG}$ is sufficient to decrease insoluble polyQ aggregation by 2-fold without a significant impact on 74Q levels in murine N2a cells. MS validated Ala mis-incorporation in the polyQ tract in cells expressing $tRNA^{Ala}_{CUG}$, confirming that the inhibition of insoluble polyQ aggregates was caused by mis-incorporation of Ala in polyQ. In contrast, the $tRNA^{Ala}_{UUG}$ variant showed little ability to alter total polyQ aggregation. In human neuroblastoma cells, we also observed that the rate of aggregate formation was significantly slower and consistently reduced over a 72 h time course in cells expressing the $tRNA^{Ala}_{CUG}$ or $tRNA^{Ser}_{CUG}$ suppressors. Since the polyQ construct contains repeating CAG codons, we were not surprised to find that the CUG anticodon is more impactful than the UUG anticodon for both Ser and Ala missense suppressors.

Related studies have identified other routes to impact polyQ aggregation through reducing translation fidelity. Deletion of a tRNA-modifying enzyme was shown to significantly reduce polyQ protein aggregates. In tRNAs, U54 is converted to 5-methyl uridine (m^5U) by TRMT2A.[72] HEK293T cells with a TRMT2A knockdown had a lower abundance of 103Q insoluble aggregates. Studies using a sensitive luminescent reporter showed elevated mis-incorporation of Glu at Gln codons in the cells. Like our suppressor tRNAs, the TRMT2A-silenced cells displayed no obvious phenotypic defects and cell growth was similar to wild-type cells.[20,21] Thus, mis-incorporation generated by a tRNA or by other genetic modifications can reduce translational fidelity at Gln codons to suppress polyQ aggregation. Our future studies will investigate the potential for synergy between suppressor tRNAs and TRMT2A silencing in resolving polyQ aggregation.

Although $tRNA^{Ala}_{CUG}$ was able to decrease the total aggregate level and insoluble aggregates specifically, the effect of Ala mis-incorporation on soluble polyQ aggregation was negligible. Conversely, the $tRNA^{Ser}_{UUG}$ suppressor was able to modestly reduce insoluble and soluble aggregates with no impact on the production of the wild-type EGFP-23Q. Although both insoluble fibrils and soluble polyQ aggregates in HD interact with a wide range of proteins, it is still debated which class of aggregates is the major cause of HD pathology.[73] Neurons expressing HTTexon1-97Q showed reduced cell viability and enhanced cytotoxicity compared to neurons expressing HTTexon-25Q.[74] The same study investigated polyQ aggregation kinetics and found that expanded polyQ generates a dominant fraction of large amyloid-like insoluble aggregates that steadily accumulate over days, while smaller polyQ oligomers form rapidly and then decay to exceedingly low levels after a period of hours.[74] Conversely, other studies suggest that the insoluble aggregates sequester more toxic soluble oligomers.[53,75–77] In future work, our missense suppressor tRNAs may be able to provide more insight on the role of soluble and insoluble polyQ aggregates in clinically relevant model systems. Since $tRNA^{Ser}_{CUG}$ reduces polyQ and aggregate levels, $tRNA^{Ser}_{UUG}$ moderately inhibits both soluble and insoluble polyQ aggregation, and $tRNA^{Ala}_{CUG}$ suppresses just insoluble polyQ aggregation, expressing each suppressor in differentiated and patient-derived neurons or animal models will

enable the definition of the role of soluble and insoluble aggregates in neurodegeneration and HD pathology.

Therapeutic potential of tRNA missense suppressors

Although there is no cure for HD yet, current promising therapeutic approaches include ASOs and small interfering RNAs (siRNAs) that target the HTT mRNA. ASOs are DNA oligomers that bind HTT pre-mRNA and block translation or target the polyQ mRNA for degradation. In undifferentiated cells expressing EGFP-53Q and differentiated neurons expressing EGFP-102Q, transfection of an ASO targeting the first 20 bases following the translation initiation site of HTT was able to inhibit EGFP-polyQ protein production. Moreover, the frequency of cells expressing EGFP-53Q aggregates was reduced from 8.3% to 0%.[78] In a related study, an ASO consisting of seven CUG repeats complementary to the polyQ mRNA was effective at inhibiting HTT transcript levels by 81% in patient-derived fibroblasts.[79] Similarly, siRNAs designed to target mHTT were successful in reducing aggregation in the HEK293T cells expressing mHTT-Q66.[80] Protein aggregation was reduced by ∼7-fold of that observed in the cells treated with a scrambled control.[80] In comparison, we found that the $tRNA^{Ala}_{CUG}$ suppressor inhibited aggregation by 2-fold and the $tRNA^{Ser}_{CUG}$ suppressor reduced 74Q production by 2-fold and nearly eliminated polyQ aggregation in murine cells and significantly inhibited aggregation kinetics in human cells.

Our work demonstrates that missense suppressor tRNAs are leads toward urgently needed HD therapies and represent a new direction in the emerging field of tRNA medicine.[34,35,81] Indeed, nonsense-suppressor tRNAs are being harnessed to ameliorate the phenotypes of several genetic disorders caused by premature termination codons.[82,83] Although the application of missense suppressor tRNAs to therapeutics is a novel route to tRNA medicine, recent studies have already demonstrated their ability to restore partial function of a CAPN3 R490Q pathogenic variant that causes limb-girdle muscular dystrophy.[33] Determining a therapeutic window wherein the level of suppression produces enough wild-type protein from a disease-causing allele is critical for the efficacy of tRNA-based therapies. Moreover, tRNAs must confer clinical benefits without inducing proteotoxic stress that overwhelms the protein quality control machinery in the cell. Our data show that tRNAs can inhibit polyQ protein production and aggregation that causes HD with no cytotoxic effects or impact on cell growth. Because the $tRNA^{Ser}_{CUG}$ variants inhibited both polyQ production and aggregation without inhibiting global protein synthesis, this tRNA will be an important lead toward novel HD therapies. The $tRNA^{Ala}_{CUG}$ variant is also an excellent candidate for further development of missense-suppressor therapies, and Ala mis-incorporation may be less toxic or damaging to the proteome compared to others forms of missense suppression.[29] While our studies in neuroblastoma cell models of HD are promising, future studies will focus on clinically relevant patient-derived and animal models of HD. Therein, we will reassess the potential for Gln-misreading tRNAs to cause toxic effects or phenotypic defects since tRNA expression or missense-suppression levels may differ across model systems.

Crucial areas for further exploration of tRNA medicine involve elucidating tissue-specific expression and efficient delivery methods for suppressor tRNAs. We recently reviewed tRNA delivery approaches, which include viral vectors and lipid nanoparticles.[35] There is particular interest in the delivery of non-integrating tRNA genes with adeno-associated viral vectors (AAVs). Indeed, AAV9 was already successfully used to deliver nonsense-suppressor tRNA to the mouse, which showed efficacy up to 6 months.[84] AAV9 was also used to deliver a gene therapy for spinal muscular atrophy that was effective in producing wild-type protein for up to 6 years in humans, eliminating the need for ventilation.[85] AAV efficacy was shown for up to 10 years in humans[86] and 15 years in primates.[87] Other AAVs, such as AAV-PHP.eB, demonstrated enhanced delivery to the brain in C57BL/6J mice,[88] making HD an accessible disease for tRNA therapy. Indeed, mHTT-targeting siRNAs can also be delivered to the brain with exosomes,[89] and ASOs for HD have reached clinical trials.[10] Promising HD therapies currently in clinical trials (e.g., AMT-130 and tominersen), including silencing RNAs or ASOs, cannot discriminate the normal from the expanded polyQ proteins; however, the ability to reduce expanded polyQ levels has clinical benefit[12] despite off-target effects. Similar to our tRNA approach, we anticipate that the off-target impacts will be tolerable to cells and that the therapeutic benefit of suppressing expanded HTT will outweigh potential toxicity from off-target mis-incorporation.

Our work represents a significant new approach toward realizing the objectives of missense suppressor tRNA-based therapies by identifying and characterizing missense suppressors that are well tolerated and effective at inhibiting polyQ aggregation in mammalian cells. This approach has the potential to alleviate the phenotypes of not only HD but other polyQ diseases such as SCA1, -2, -6, -7, and -17, Machado-Joseph disease (MJD/SCA3), and dentatorubral-pallidoluysian atrophy (DRPLA), for which no cures exist.

Conclusion

We assessed Ser and Ala missense suppressor tRNAs to determine their impact on polyQ protein production and aggregation. We identified $tRNA^{Ala}_{CUG}$ as an effective missense suppressor that significantly reduced the formation of insoluble 74Q aggregates without inducing cytotoxicity or impacting cell growth. Reduced polyQ aggregation was achieved through mis-incorporation of Ala into the expanded polyQ tract, which we confirmed by mass spectrometry. Our findings also revealed differential effects of missense suppressor tRNAs on polyQ protein production and polyQ aggregation. Notably, $tRNA^{Ser}_{CUG}$ inhibited polyQ production in both murine and human neuroblastoma cells, and $tRNA^{Ala}_{CUG}$ was somewhat more impactful in human as compared to murine cells, indicating the importance of the cellular context in the application of tRNA-based therapies. Furthermore, our study contributes to the growing body of evidence supporting the therapeutic potential of tRNAs for genetic diseases. Our findings hold promise for addressing a wide spectrum of genetic diseases caused by expanded polyQ repeats or missense mutations.

MATERIALS AND METHODS

Plasmids and cloning

pEGFP-derived HTTexon1 (MKAFESLKSF-[polyQ]-P11-QLPQPP) expression plasmids were purchased from Addgene (pEGFP-Q23 #40261, pEGFP-Q74 #40262). The tRNA alanine and serine genes were selected using tRNA activity-level predictions based on data from human cells.[34,38] The tRNA genes of interest were amplified from the genomic DNA of HEK (HEK293T) cells via polymerase chain reaction (PCR) following the PfuUltra II polymerase protocol (Agilent, CA, USA). Primers were designed to amplify ∼300 base pairs up- and downstream of the tRNA genes of interest. Anticodon variants were introduced in PCR fragments using overlap extension PCR. PCR products were purified from a 1.5% Tris-acetate-EDTA (TAE) agarose gel with ethidium bromide using the GenepHlow Gel/PCR Extraction Kit (GeneAid, New Taipei City, Taiwan). tRNA expression cassettes were inserted at the *Pci*I (New England Biolabs [NEB], Ipswich, MA, USA) restriction site in pEGFP-Q23 or pEGFP-Q74-derived plasmids and ligated with T4 DNA ligase (NEB). A WT-PAN plasmid[90] (Addgene #99638) encoding a GFP-mCherry fusion protein with no additional tRNA or with the $tRNA^{Ala}$ or $tRNA^{Ala}_{CUG}$ mutant genes incorporated at the *Pci*I site was used for studies of GFP-mCherry production. Plasmid DNA for mammalian cell transfection was purified by Midi-Prep (GeneAid) from 100 mL *E. coli* DH5α cultures grown at 37°C for 16 h to A_{600} > 1.0. DNA concentrations were measured using a Nanodrop 2000C (Thermo Fisher Scientific). All plasmid sequences were verified by Sanger sequencing (Azenta US, South Plainfield, NJ, USA), and PCR primers are listed in Table S2.

Cell culture and fluorescence microscopy

Cell culture experiments were performed in mouse N2a neuroblastoma cells (ATCC #CCL-131) and human SH-SY5Y neuroblastoma cells (SH-SY5Y; ATCC #CRL-226) grown at 37°C with humidity and 5% CO_2. N2a and SH-SY5Y cells were cultured in high-glucose Dulbecco's modified Eagle medium (DMEM; 4.5 g/L glucose; Gibco by Life Technologies, Carlsbad, CA) containing 10% fetal bovine serum (FBS; Gibco), and 1% penicillin-streptomycin (P/S; P: 100 IU/mL; S: 100 IU/mL; Wisent Bioproducts, Montreal, QC, Canada). All plasmid transfections were performed using Lipofectamine 3000 transfection reagent (Invitrogen) following the manufacturer's instructions for the appropriate plate size. Fluorescent images were taken on an EVOS FL auto-fluorescent microscope (Thermo Fisher Scientific). GFP fluorescence was visualized using the EVOS LED GFP filter cube (470 ± 22 nm excitation, 510 ± 42 nm emission) to capture green fluorescence, and mCherry fluorescence was visualized using the EVOS LED RFP filter cube (531 ± 40 nm excitation, 593 ± 40 nm emission). Images were captured at 24, 48, and/or 72 h after transfection as indicated and quantitated by thresholding analysis using a custom ImageJ/Fiji script.[27] As we and others established previously,[27,51] the threshold to define protein aggregates (Figure S5) was set to 18 standard deviations above the mean fluorescent pixel value.

Cell harvest and lysis

Cells at 70% confluency were plated in 6-well plates and transfected as above. At 72 h post-transfection, media were aspirated, and cells were lifted in phosphate-buffered saline (PBS; 137 mM NaCl, 2.7 mM KCl, 10 mM Na_2HPO_4, 1.8 mM KH_2PO_4 [pH 7.4]) + 10 mM ethylenediaminetetraacetic acid (EDTA) after 10 min of incubation at 37°C with humidity and 5% CO_2. Cells were resuspended and transferred to a sterile 1.5 mL Eppendorf tube and centrifuged at 500 × *g* for 10 min at room temperature. The supernatant was aspirated, and cell pellets were used immediately or stored at −80°C until cell lysis. Cell lysis was performed on ice: each cell pellet was resuspended in 50 μL of mammalian cell lysis buffer (50 mM Na_2HPO_4, 1 mM Na_4P2O_7, 20 mM NaF, 2 mM EDTA, 2 mM EGTA, 1 mM Triton X-100, 1 mM dithiothreitol, 0.3 mM phenylmethylsulfonyl fluoride, and 1 tablet/10 mL complete mini EDTA-free Protease Inhibitor Cocktail). Resuspended cells were incubated on ice for 5 min and then centrifuged at 21.1 × *g* at 4°C for 20 min. Supernatants were transferred into fresh, sterile 1.5 mL Eppendorf tubes. The Pierce bicinchoninic acid (BCA) assay (Thermo Fisher Scientific) was used to determine lysate protein concentrations to calculate the appropriate loading volumes after dilution with 3× sodium dodecyl sulfate (SDS) loading dye (0.5 M Tris-HCl [pH 6.8]; 1.12 M sucrose; 0.025% bromophenol blue; 3.8% SDS) for western blotting.

Western blotting

Following cell harvest and lysis, 15 μg of protein from each lysate was separated on SDS-polyacrylamide gel electrophoresis (SDS-PAGE) with 12% acrylamide and including protein standards (PM008-0500, FroggaBio, Concord, ON, Canada) for size determination. After SDS-PAGE, proteins were transferred to a polyvinylidene fluoride (PVDF) membrane using a Trans-Blot Turbo Transfer System (25 V, 1.3 A constant for 20 min; Bio-Rad). Membranes were incubated in blocking solution (5% bovine serum albumin [BSA], 0.1% Tween 20, 1× Tris-buffered saline [TBS]) for 1 h at room temperature. Membranes were then incubated with primary antibodies at 1:500 (α-GFP, Abcam, ab32146; α-vinculin, NEB, E1E9V) in blocking solution overnight at 4°C. The following day, membranes were washed for 3 × 10 min in BSA wash solution (1% BSA, 0.1% Tween 20, 1% TBS) and then incubated with IRDye 800CW donkey anti-rabbit (Li-Cor, 926-32213; 1:10,000 dilution) for GFP or IRDye 680RD goat anti-rabbit (Li-Cor, 926-68071; 1:5,000 dilution) for vinculin for 2 h at room temperature. Membranes were washed for 3 × 10 min with 1× TBS with 0.1% Tween 20, followed by one wash for 10 min in 1× TBS. Membranes were imaged using fluorescence on a ChemiDoc MP imager (Bio-Rad). For studies of GFP-mCherry production, cell lysates were probed with specific antibodies for primary GFP and secondary IRDye800CW donkey anti-rabbit antibodies as above; the vinculin (anti-vinculin produced in mouse, V9131, Sigma) loading control was visualized using chemiluminescence as described before.[31] Briefly, a secondary ECL anti-mouse immunoglobulin (Ig)G, horseradish peroxidase-linked whole antibody (from sheep, GPR NXA931V, GE Healthcare UK) was used for detection of anti-vinculin, and chemiluminescence was conducted using the Clarity Western Blotting ECL Substrate (Bio-Rad) per the manufacturer's instructions and imaged using a ChemiDoc MP imager (Bio-Rad). To determine

p-eIF2α levels, specific antibodies for eIF2α (Invitrogen, anti-EIF2α, #AHO0802), p-eIF2α (Abcam, ab32157, anti-EIF2S51, phospho-S51), and a vinculin loading control were used as above. The IRDye 800CW donkey anti-rabbit secondary antibody was used to detect the eIF2α antibodies.

Protein synthesis assay

Protein synthesis was measured using the SUnSET method, which measures the incorporation of puromycin in nascent peptide chains. At 72 h after transfection, SH-SY5Y cells were incubated in puromycin treatment media: 5 μg/mL puromycin in DMEM (10% FBS, 1% P/S). After a 1 h incubation at 37°C, puromycin treatment was removed and cells harvested with PBS for cell lysis as above. Samples of 40 μg of protein were separated using 10% SDS-PAGE. Proteins were transferred to a PVDF membrane using a Trans-Blot Turbo Transfer System (25 V, 1.3 A, constant for 25 min; Bio-Rad) and subsequently incubated in TBST buffer containing 5% BSA for 1 h at room temperature. Membranes were then incubated at 4°C overnight with a monoclonal puromycin antibody (clone 12D10, EMD Millipore, Temecula, CA, USA, diluted 1:500 in TBST and 5% BSA w/v) and then washed three times with TBST and 1% BSA for 10 min each the following day. Membranes were incubated for 2 h in TBST containing 3% skim milk plus a secondary mouse antibody (Sigma-Aldrich, 1:5000) and then washed three times with TBST for 15 min each. Membranes were visualized on the Bio-Rad ChemiDoc imaging system. The total lane density was analyzed using ImageJ.

SDD-AGE

N2a cells were transfected, harvested, and lysed as above. Cell lysate containing 15 μg of protein was diluted in 3× loading dye and loaded and separated on a 1.5% TAE agarose gel supplemented with 0.1% SDS according to established protocols.[91] Proteins were transferred to a PVDF membrane by capillary electrophoresis overnight using 1× TAE (40 mM Tris-base, 20 mM acetic acid, 1 mM EDTA) with 0.1% SDS. EGFP-tagged polyQ aggregates were visualized by western blotting with the anti-GFP antibody as above and imaged using fluorescence on a ChemiDoc MP imager (Bio-Rad).

Triton X-100 assay

To quantify insoluble protein aggregates, a membrane detergent assay with Triton X-100 was performed following established protocols. Initial images were captured using the EVOS microscope 72 h after transfection in a 96-well plate. Cells were then treated with DMEM containing 0.25% Triton X-100 and incubated at 37°C with humidity and 5% CO_2. After 40 min, images were captured again from the same location. The size of insoluble aggregates remaining was quantified in ImageJ/Fiji using thresholding analysis.

Cytotoxicity and cell growth assays

The CytoTox-Glo assay (Promega, WI, USA) was used to measure cytotoxicity in N2a cells according to the manufacturer's instructions. A 50 μL aliquot of assay reagent was added to each well, and an initial luminescence reading was taken using the Synergy H1 Plate Reader (BioTek, VT, USA). Then, 50 μL of assay buffer with digitonin was added to each well, and a final luminescence reading was taken. The initial luminescence reading quantifies the population of dead cells in each well, and the addition of digitonin determines the total number of cells present in each well. Cell proliferation was measured using the Cell Counting Kit (CCK)-8 (Sigma-Aldrich, 96992) assay, which is based on the conversion of water-soluble tetrazolium salt, WST-8 (2-(2-methoxy-4-nitrophenyl)-3-(4-nitrophenyl)-5-(2,4-disulfophenyl)-2H-tetrazolium, monosodium salt), to a water-soluble formazan dye upon reduction in the presence of an electron carrier by dehydrogenases in viable cells. SH-SY5Y cells were transfected in 96-well plates with Lipofectamine 3000 (Invitrogen, Thermo Fisher Scientific) according to the manufacturer's protocol. At 6, 24, 48, and 72 h after transfection, cells were treated with 10 μL of the CCK-8 reagent and then incubated for 4 h at 37°C with 5% CO_2 and humidity. Absorbance was measured at A = 450 nm using the Cytation C10 imaging plate reader (Agilent BioTek).

MS

EGFP protein was immunoprecipitated from N2a cells expressing EGFP-HTTexon1 23Q or 74Q with either no additional tRNA or with $tRNA^{Ala}_{CUG}$ co-expressed. At 72 h post-transfection, 10 cm plates of transfected cells in $n = 3$ biological replicates were harvested for each cell line and lysed with ice-cold lysis buffer (10 mM Tris/Cl [pH 7.5], 150 mM NaCl, 0.5 mM EDTA, 0.5% nonidet P40 substitute [pH 4]). EGFP-polyQ was purified through immunoprecipitation using the GFP-Trap Agarose kit (Chromotek, Munich, Germany) according to the manufacturer's instructions. Purified EGFP-polyQ protein was diluted with 2× SDS-running buffer and separated using SDS-PAGE with 10% acrylamide. Bands corresponding to EGFP-polyQ were excised from the Coomassie-stained gel. Excised bands were stored in 5% acetic acid and submitted for LC-MS/MS analysis to Bioinformatics Solutions (Waterloo, ON, Canada). The protein samples were digested with pepsin, and a trapped ion mobility spectroscopy time-of-flight (*tims*TOF) mass spectrometer (Bruker Daltronics, Bremen, Germany) was used to identify alanine mis-incorporation in EGFP-23Q and EGFP-74Q proteins. Detailed MS methods can be found in the supplemental information.

DATA AND CODE AVAILABILITY

Mass spectra were deposited in the PRIDE database. ProteomeXchange accession: PXD053115; Project web page: http://www.ebi.ac.uk/pride/archive/projects/PXD053115; FTP download: https://ftp.pride.ebi.ac.uk/pride/data/archive/2025/01/PXD053115.

ACKNOWLEDGMENTS

We are grateful to Ilka Heinemann for insightful discussions and suggestions and to Jenica Kakadia for immunoblotting expertise. This work was supported by the Natural Sciences and Engineering Research Council of Canada (04282 and 580241 to P.O'D.), Canada Research Chairs (232341 to P.O'D.), the Canadian Institutes of Health Research (165985 to P.O'D.), and a Schulich School of Medicine & Dentistry Collaborative Research Seed Grant (to T.B.B. and P.O'D.). P.O'D. is also supported by the Huntington Society of Canada Research Chair at Western University.

AUTHOR CONTRIBUTIONS

Conceptualization, R.T., T.M.I.B., F.H., A.V., and P.O'D.; data curation, R.T., T.M.I.B., S.S., K.S.H., and P.O'D.; formal analysis, R.T., T.M.I.B., and K.S.H.; investigation, R.T., T.M.I.B., T.B.B., and P.O'D.; methodology, R.T., T.M.I.B., F.H., and P.O'D.; validation,

R.T. and T.M.I.B.; visualization, R.T., T.M.I.B., and P.O'D.; writing – original draft, R.T. and P.O'D.; writing – review & editing, R.T., A.V., and P.O'D.; funding acquisition, T.B.B. and P.O'D.; supervision, T.B.B. and P.O'D.; project administration, P.O'D.; resources, P.O'D.

DECLARATION OF INTERESTS

The authors declare no conflicts of interest.

SUPPLEMENTAL INFORMATION

Supplemental information can be found online at https://doi.org/10.1016/j.omtn.2024.102442.

REFERENCES

1. Orr, H.T., and Zoghbi, H.Y. (2007). Trinucleotide repeat disorders. Annu. Rev. Neurosci. *30*, 575–621. https://doi.org/10.1146/annurev.neuro.29.051605.113042.
2. Kremer, B., Goldberg, P., Andrew, S.E., Theilmann, J., Telenius, H., Zeisler, J., Squitieri, F., Lin, B., Bassett, A., Almqvist, E., et al. (1994). A worldwide study of the Huntington's disease mutation. The sensitivity and specificity of measuring CAG repeats. N. Engl. J. Med. *330*, 1401–1406. https://doi.org/10.1056/nejm199405193302001.
3. Genetic Modifiers of Huntington's Disease GeM-HD Consortium Electronic address gusella@helixmghharvardedu; Genetic Modifiers of Huntington's Disease GeM-HD Consortium (2019). CAG Repeat Not Polyglutamine Length Determines Timing of Huntington's Disease Onset. Cell *178*, 887–900.e14. https://doi.org/10.1016/j.cell.2019.06.036.
4. Langbehn, D.R.; Registry Investigators of the European Huntington Disease Network (2022). Longer CAG repeat length is associated with shorter survival after disease onset in Huntington disease. Am. J. Hum. Genet. *109*, 172–179. https://doi.org/10.1016/j.ajhg.2021.12.002.
5. Wilton, D.K., and Stevens, B. (2020). The contribution of glial cells to Huntington's disease pathogenesis. Neurobiol. Dis. *143*, 104963. https://doi.org/10.1016/j.nbd.2020.104963.
6. Schulte, J., and Littleton, J.T. (2011). The biological function of the Huntingtin protein and its relevance to Huntington's Disease pathology. Curr. Trends Neurol. *5*, 65–78.
7. Kang, H., Vázquez, F.X., Zhang, L., Das, P., Toledo-Sherman, L., Luan, B., Levitt, M., and Zhou, R. (2017). Emerging β-Sheet Rich Conformations in Supercompact Huntingtin Exon-1 Mutant Structures. J. Am. Chem. Soc. *139*, 8820–8827. https://doi.org/10.1021/jacs.7b00838.
8. Mikhaylova, E.R., Lazarev, V.F., Nikotina, A.D., Margulis, B.A., and Guzhova, I.V. (2016). Glyceraldehyde 3-phosphate dehydrogenase augments the intercellular transmission and toxicity of polyglutamine aggregates in a cell model of Huntington disease. J. Neurochem. *136*, 1052–1063. https://doi.org/10.1111/jnc.13463.
9. Reiner, A., Dragatsis, I., and Dietrich, P. (2011). Genetics and neuropathology of Huntington's disease. Int. Rev. Neurobiol. *98*, 325–372. https://doi.org/10.1016/b978-0-12-381328-2.00014-6.
10. Rook, M.E., and Southwell, A.L. (2022). Antisense Oligonucleotide Therapy: From Design to the Huntington Disease Clinic. BioDrugs *36*, 105–119. https://doi.org/10.1007/s40259-022-00519-9.
11. Tabrizi, S.J., Leavitt, B.R., Landwehrmeyer, G.B., Wild, E.J., Saft, C., Barker, R.A., Blair, N.F., Craufurd, D., Priller, J., Rickards, H., et al. (2019). Targeting Huntingtin Expression in Patients with Huntington's Disease. N. Engl. J. Med. *380*, 2307–2316. https://doi.org/10.1056/NEJMoa1900907.
12. Estevez-Fraga, C., Tabrizi, S.J., and Wild, E.J. (2024). Huntington's Disease Clinical Trials Corner: March 2024. J. Huntingtons Dis. *13*, 1–14. https://doi.org/10.3233/JHD-240017.
13. Miniarikova, J., Zanella, I., Huseinovic, A., van der Zon, T., Hanemaaijer, E., Martier, R., Koornneef, A., Southwell, A.L., Hayden, M.R., van Deventer, S.J., et al. (2016). Design, Characterization, and Lead Selection of Therapeutic miRNAs Targeting Huntingtin for Development of Gene Therapy for Huntington's Disease. Mol. Ther. Nucleic Acids *5*, e297. https://doi.org/10.1038/mtna.2016.7.
14. Peng, S.I., Leong, L.I., Sun, J.K.L., Chen, Z.S., Chow, H.M., and Chan, H.Y.E. (2022). A peptide inhibitor that rescues polyglutamine-induced synaptic defects and cell death through suppressing RNA and protein toxicities. Mol. Ther. Nucleic Acids *29*, 102–115. https://doi.org/10.1016/j.omtn.2022.06.004.
15. Walters, R.H., and Murphy, R.M. (2011). Aggregation kinetics of interrupted polyglutamine peptides. J. Mol. Biol. *412*, 505–519. https://doi.org/10.1016/j.jmb.2011.07.003.
16. Thakur, A.K., Yang, W., and Wetzel, R. (2004). Inhibition of polyglutamine aggregate cytotoxicity by a structure-based elongation inhibitor. Faseb. J. *18*, 923–925. https://doi.org/10.1096/fj.03-1238fje.
17. Jayaraman, M., Kodali, R., and Wetzel, R. (2009). The impact of ataxin-1-like histidine insertions on polyglutamine aggregation. Protein Eng. Des. Sel. *22*, 469–478. https://doi.org/10.1093/protein/gzp023.
18. Girstmair, H., Saffert, P., Rode, S., Czech, A., Holland, G., Bannert, N., and Ignatova, Z. (2013). Depletion of cognate charged transfer RNA causes translational frameshifting within the expanded CAG stretch in huntingtin. Cell Rep. *3*, 148–159. https://doi.org/10.1016/j.celrep.2012.12.019.
19. Saffert, P., Adamla, F., Schieweck, R., Atkins, J.F., and Ignatova, Z. (2016). An Expanded CAG Repeat in Huntingtin Causes +1 Frameshifting. J. Biol. Chem. *291*, 18505–18513. https://doi.org/10.1074/jbc.M116.744326.
20. Margreiter, M.A., Witzenberger, M., Wasser, Y., Davydova, E., Janowski, R., Metz, J., Habib, P., Sahnoun, S.E.M., Sobisch, C., Poma, B., et al. (2022). Small-molecule modulators of TRMT2A decrease PolyQ aggregation and PolyQ-induced cell death. Comput. Struct. Biotechnol. J. *20*, 443–458. https://doi.org/10.1016/j.csbj.2021.12.029.
21. VoSSfeldt, H., Butzlaff, M., PrüSSing, K., Ní Chárthaigh, R.A., Karsten, P., Lankes, A., Hamm, S., Simons, M., Adryan, B., Schulz, J.B., and Voigt, A. (2012). Large-scale screen for modifiers of ataxin-3-derived polyglutamine-induced toxicity in Drosophila. PLoS One *7*, e47452. https://doi.org/10.1371/journal.pone.0047452.
22. Marchionini, D.M., Liu, J.P., Ambesi-Impiombato, A., Kerker, K., Cirillo, K., Bansal, M., Mushlin, R., Brunner, D., Ramboz, S., Kwan, M., et al. (2022). Benefits of global mutant huntingtin lowering diminish over time in a Huntington's disease mouse model. JCI Insight *7*, e161769. https://doi.org/10.1172/jci.insight.161769.
23. Tabrizi, S.J., Ghosh, R., and Leavitt, B.R. (2019). Huntingtin Lowering Strategies for Disease Modification in Huntington's Disease. Neuron *101*, 801–819. https://doi.org/10.1016/j.neuron.2019.01.039.
24. O'Donoghue, P., and Luthey-Schulten, Z. (2003). On the evolution of structure in aminoacyl-tRNA synthetases. Microbiol. Mol. Biol. Rev. *67*, 550–573. https://doi.org/10.1128/mmbr.67.4.550-573.2003.
25. Giegé, R., Sissler, M., and Florentz, C. (1998). Universal rules and idiosyncratic features in tRNA identity. Nucleic Acids Res. *26*, 5017–5035. https://doi.org/10.1093/nar/26.22.5017.
26. Giegé, R., and Eriani, G. (2023). The tRNA identity landscape for aminoacylation and beyond. Nucleic Acids Res. *51*, 1528–1570. https://doi.org/10.1093/nar/gkad007.
27. Lant, J.T., Kiri, R., Duennwald, M.L., and O'Donoghue, P. (2021). Formation and persistence of polyglutamine aggregates in mistranslating cells. Nucleic Acids Res. *49*, 11883–11899. https://doi.org/10.1093/nar/gkab898.
28. Hasan, F., Lant, J.T., and O'Donoghue, P. (2023). Perseverance of protein homeostasis despite mistranslation of glycine codons with alanine. Philos. Trans. R. Soc. Lond. B Biol. Sci. *378*, 20220029. https://doi.org/10.1098/rstb.2022.0029.
29. Davey-Young, J., Hasan, F., Tennakoon, R., Rozik, P., Moore, H., Hall, P., Cozma, E., Genereaux, J., Hoffman, K.S., Chan, P.P., et al. (2024). Mistranslating the genetic code with leucine in yeast and mammalian cells. RNA Biol. *21*, 1–23. https://doi.org/10.1080/15476286.2024.2340297.
30. Lant, J.T., Berg, M.D., Heinemann, I.U., Brandl, C.J., and O'Donoghue, P. (2019). Pathways to disease from natural variations in human cytoplasmic tRNAs. J. Biol. Chem. *294*, 5294–5308. https://doi.org/10.1074/jbc.REV118.002982.
31. Lant, J.T., Hasan, F., Briggs, J., Heinemann, I.U., and O'Donoghue, P. (2023). Genetic Interaction of tRNA-Dependent Mistranslation with Fused in Sarcoma Protein Aggregates. Genes *14*, 518. https://doi.org/10.3390/genes14020518.

32. Bily, T.M.I., Heinemann, I.U., and O'Donoghue, P. (2024). Missense suppressor tRNA therapeutics correct disease-causing alleles by misreading the genetic code. Mol. Ther. *32*, 273–274. https://doi.org/10.1016/j.ymthe.2024.01.001.

33. Hou, Y., Zhang, W., McGilvray, P.T., Sobczyk, M., Wang, T., Weng, S.H.S., Huff, A., Huang, S., Pena, N., Katanski, C.D., and Pan, T. (2024). Engineered mischarged transfer RNAs for correcting pathogenic missense mutations. Mol. Ther. *32*, 352–371. https://doi.org/10.1016/j.ymthe.2023.12.014.

34. Thornlow, B.P., Armstrong, J., Holmes, A.D., Howard, J.M., Corbett-Detig, R.B., and Lowe, T.M. (2020). Predicting transfer RNA gene activity from sequence and genome context. Genome Res. *30*, 85–94. https://doi.org/10.1101/gr.256164.119.

35. Ward, C., Beharry, A., Tennakoon, R., Rozik, P., Wilhelm, S.D.P., Heinemann, I.U., and O'Donoghue, P. (2024). Mechanisms and Delivery of tRNA Therapeutics. Chem. Rev. *124*, 7976–8008. https://doi.org/10.1021/acs.chemrev.4c00142.

36. Zhou, D.H., Lee, J., Frankenberger, C., Geslain, R., Rosner, M., and Pan, T. (2012). Anti-tumor effects of an engineered "killer" transfer RNA. Biochem. Biophys. Res. Commun. *427*, 148–153. https://doi.org/10.1016/j.bbrc.2012.09.028.

37. Lustig, F., Elias, P., Axberg, T., Samuelsson, T., Tittawella, I., and Lagerkvist, U. (1981). Codon reading and translational error. Reading of the glutamine and lysine codons during protein synthesis in vitro. J. Biol. Chem. *256*, 2635–2643.

38. Chan, P.P., and Lowe, T.M. (2016). GtRNAdb 2.0: an expanded database of transfer RNA genes identified in complete and draft genomes. Nucleic Acids Res. *44*, D184–D189. https://doi.org/10.1093/nar/gkv1309.

39. Hrabeta-Robinson, E., Marcus, E., Cozen, A.E., Phizicky, E.M., and Lowe, T.M. (2017). High-Throughput Small RNA Sequencing Enhanced by AlkB-Facilitated RNA de-Methylation (ARM-Seq). Methods Mol. Biol. *1562*, 231–243. https://doi.org/10.1007/978-1-4939-6807-7_15.

40. ENCODE Project Consortium (2012). An integrated encyclopedia of DNA elements in the human genome. Nature *489*, 57–74. https://doi.org/10.1038/nature11247.

41. Parisien, M., Wang, X., and Pan, T. (2013). Diversity of human tRNA genes from the 1000-genomes project. RNA Biol. *10*, 1853–1867. https://doi.org/10.4161/rna.27361.

42. Haeussler, M., Zweig, A.S., Tyner, C., Speir, M.L., Rosenbloom, K.R., Raney, B.J., Lee, C.M., Lee, B.T., Hinrichs, A.S., Gonzalez, J.N., et al. (2019). The UCSC Genome Browser database: 2019 update. Nucleic Acids Res. *47*, D853–D858. https://doi.org/10.1093/nar/gky1095.

43. GTEx Consortium (2013). The Genotype-Tissue Expression (GTEx) project. Nat. Genet. *45*, 580–585. https://doi.org/10.1038/ng.2653.

44. Maxan, A., Sciacca, G., Alpaugh, M., Tao, Z., Breger, L., Dehay, B., Ling, Z., Chuan, Q., Cisbani, G., Masnata, M., et al. (2020). Use of adeno-associated virus-mediated delivery of mutant huntingtin to study the spreading capacity of the protein in mice and non-human primates. Neurobiol. Dis. *141*, 104951. https://doi.org/10.1016/j.nbd.2020.104951.

45. Zhang, Y., Leavitt, B.R., van Raamsdonk, J.M., Dragatsis, I., Goldowitz, D., MacDonald, M.E., Hayden, M.R., and Friedlander, R.M. (2006). Huntingtin inhibits caspase-3 activation. EMBO J. *25*, 5896–5906. https://doi.org/10.1038/sj.emboj.7601445.

46. Cisbani, G., and Cicchetti, F. (2012). An in vitro perspective on the molecular mechanisms underlying mutant huntingtin protein toxicity. Cell Death Dis. *3*, e382. https://doi.org/10.1038/cddis.2012.121.

47. Geslain, R., Cubells, L., Bori-Sanz, T., Alvarez-Medina, R., Rossell, D., Martí, E., and Ribas de Pouplana, L. (2010). Chimeric tRNAs as tools to induce proteome damage and identify components of stress responses. Nucleic Acids Res. *38*, e30. https://doi.org/10.1093/nar/gkp1083.

48. Schmidt, E.K., Clavarino, G., Ceppi, M., and Pierre, P. (2009). SUnSET, a nonradioactive method to monitor protein synthesis. Nat. Methods *6*, 275–277. https://doi.org/10.1038/nmeth.1314.

49. Zhang, H., and Ling, J. (2024). Serine mistranslation induces the integrated stress response without accumulation of uncharged tRNAs. Preprint at bioRxiv. https://doi.org/10.1101/2024.02.04.578812.

50. Wang, X., and Proud, C.G. (2022). The role of eIF2 phosphorylation in cell and organismal physiology: new roles for well-known actors. Biochem. J. *479*, 1059–1082. https://doi.org/10.1042/BCJ20220068.

51. Klickstein, J.A., Mukkavalli, S., and Raman, M. (2020). AggreCount: an unbiased image analysis tool for identifying and quantifying cellular aggregates in a spatially defined manner. J. Biol. Chem. *295*, 17672–17683. https://doi.org/10.1074/jbc.RA120.015398.

52. Titus, S.A., Southall, N., Marugan, J., Austin, C.P., and Zheng, W. (2012). High-Throughput Multiplexed Quantitation of Protein Aggregation and Cytotoxicity in a Huntington's Disease Model. Curr. Chem. Genom. *6*, 79–86. https://doi.org/10.2174/1875397301206010079.

53. Kim, Y.E., Hosp, F., Frottin, F., Ge, H., Mann, M., Hayer-Hartl, M., and Hartl, F.U. (2016). Soluble Oligomers of PolyQ-Expanded Huntingtin Target a Multiplicity of Key Cellular Factors. Mol. Cell *63*, 951–964. https://doi.org/10.1016/j.molcel.2016.07.022.

54. Thornlow, B.P., Hough, J., Roger, J.M., Gong, H., Lowe, T.M., and Corbett-Detig, R.B. (2018). Transfer RNA genes experience exceptionally elevated mutation rates. Proc. Natl. Acad. Sci. USA *115*, 8996–9001. https://doi.org/10.1073/pnas.1801240115.

55. Capone, J.P. (1988). Modulation of the phenotypic expression of a human serine tRNA gene by 5'-flanking sequences. DNA *7*, 459–468. https://doi.org/10.1089/dna.1.1988.7.459.

56. Ross, C.A. (2002). Polyglutamine pathogenesis: emergence of unifying mechanisms for Huntington's disease and related disorders. Neuron *35*, 819–822. https://doi.org/10.1016/s0896-6273(02)00872-3.

57. Li, H., Li, S.H., Yu, Z.X., Shelbourne, P., and Li, X.J. (2001). Huntingtin aggregate-associated axonal degeneration is an early pathological event in Huntington's disease mice. J. Neurosci. *21*, 8473–8481. https://doi.org/10.1523/jneurosci.21-21-08473.2001.

58. Ferrante, R.J., Kowall, N.W., and Richardson, E.P., Jr. (1991). Proliferative and degenerative changes in striatal spiny neurons in Huntington's disease: a combined study using the section-Golgi method and calbindin D28k immunocytochemistry. J. Neurosci. *11*, 3877–3887. https://doi.org/10.1523/jneurosci.11-12-03877.1991.

59. Sotrel, A., Williams, R.S., Kaufmann, W.E., and Myers, R.H. (1993). Evidence for neuronal degeneration and dendritic plasticity in cortical pyramidal neurons of Huntington's disease: a quantitative Golgi study. Neurology *43*, 2088–2096. https://doi.org/10.1212/wnl.43.10.2088.

60. Gutekunst, C.A., Li, S.H., Yi, H., Mulroy, J.S., Kuemmerle, S., Jones, R., Rye, D., Ferrante, R.J., Hersch, S.M., and Li, X.J. (1999). Nuclear and neuropil aggregates in Huntington's disease: relationship to neuropathology. J. Neurosci. *19*, 2522–2534. https://doi.org/10.1523/jneurosci.19-07-02522.1999.

61. Weiss, K.R., Kimura, Y., Lee, W.C.M., and Littleton, J.T. (2012). Huntingtin aggregation kinetics and their pathological role in a Drosophila Huntington's disease model. Genetics *190*, 581–600. https://doi.org/10.1534/genetics.111.133710.

62. Chen, S., Ferrone, F.A., and Wetzel, R. (2002). Huntington's disease age-of-onset linked to polyglutamine aggregation nucleation. Proc. Natl. Acad. Sci. USA *99*, 11884–11889. https://doi.org/10.1073/pnas.182276099.

63. Sugaya, K., and Matsubara, S. (2012). Quantitative connection between polyglutamine aggregation kinetics and neurodegenerative process in patients with Huntington's disease. Mol. Neurodegener. *7*, 20. https://doi.org/10.1186/1750-1326-7-20.

64. Zheng, S., Clabough, E.B.D., Sarkar, S., Futter, M., Rubinsztein, D.C., and Zeitlin, S.O. (2010). Deletion of the huntingtin polyglutamine stretch enhances neuronal autophagy and longevity in mice. PLoS Genet. *6*, e1000838. https://doi.org/10.1371/journal.pgen.1000838.

65. Goldberg, Y.P., Nicholson, D.W., Rasper, D.M., Kalchman, M.A., Koide, H.B., Graham, R.K., Bromm, M., Kazemi-Esfarjani, P., Thornberry, N.A., Vaillancourt, J.P., and Hayden, M.R. (1996). Cleavage of huntingtin by apopain, a proapoptotic cysteine protease, is modulated by the polyglutamine tract. Nat. Genet. *13*, 442–449. https://doi.org/10.1038/ng0896-442.

66. Wellington, C.L., Ellerby, L.M., Hackam, A.S., Margolis, R.L., Trifiro, M.A., Singaraja, R., McCutcheon, K., Salvesen, G.S., Propp, S.S., Bromm, M., et al. (1998). Caspase cleavage of gene products associated with triplet expansion disorders generates truncated fragments containing the polyglutamine tract. J. Biol. Chem. *273*, 9158–9167. https://doi.org/10.1074/jbc.273.15.9158.

67. Reynolds, S.D., Angerer, L.M., Palis, J., Nasir, A., and Angerer, R.C. (1992). Early mRNAs, spatially restricted along the animal-vegetal axis of sea urchin embryos,

include one encoding a protein related to tolloid and BMP-1. Development *114*, 769–786. https://doi.org/10.1242/dev.114.3.769.

68. Landles, C., Sathasivam, K., Weiss, A., Woodman, B., Moffitt, H., Finkbeiner, S., Sun, B., Gafni, J., Ellerby, L.M., Trottier, Y., et al. (2010). Proteolysis of mutant huntingtin produces an exon 1 fragment that accumulates as an aggregated protein in neuronal nuclei in Huntington disease. J. Biol. Chem. *285*, 8808–8823. https://doi.org/10.1074/jbc.M109.075028.

69. Sathasivam, K., Neueder, A., Gipson, T.A., Landles, C., Benjamin, A.C., Bondulich, M.K., Smith, D.L., Faull, R.L.M., Roos, R.A.C., Howland, D., et al. (2013). Aberrant splicing of HTT generates the pathogenic exon 1 protein in Huntington disease. Proc. Natl. Acad. Sci. USA *110*, 2366–2370. https://doi.org/10.1073/pnas.1221891110.

70. Mangiarini, L., Sathasivam, K., Seller, M., Cozens, B., Harper, A., Hetherington, C., Lawton, M., Trottier, Y., Lehrach, H., Davies, S.W., and Bates, G.P. (1996). Exon 1 of the HD gene with an expanded CAG repeat is sufficient to cause a progressive neurological phenotype in transgenic mice. Cell *87*, 493–506. https://doi.org/10.1016/s0092-8674(00)81369-0.

71. Chen, M., and Wolynes, P.G. (2017). Aggregation landscapes of Huntingtin exon 1 protein fragments and the critical repeat length for the onset of Huntington's disease. Proc. Natl. Acad. Sci. USA *114*, 4406–4411. https://doi.org/10.1073/pnas.1702237114.

72. Boccaletto, P., Machnicka, M.A., Purta, E., Piatkowski, P., Baginski, B., Wirecki, T.K., de Crécy-Lagard, V., Ross, R., Limbach, P.A., Kotter, A., et al. (2018). MODOMICS: a database of RNA modification pathways. 2017 update. Nucleic Acids Res. *46*, D303–D307. https://doi.org/10.1093/nar/gkx1030.

73. Jarosińska, O.D., and Rüdiger, S.G.D. (2021). Molecular Strategies to Target Protein Aggregation in Huntington's Disease. Front. Mol. Biosci. *8*, 769184. https://doi.org/10.3389/fmolb.2021.769184.

74. Drombosky, K.W., Rode, S., Kodali, R., Jacob, T.C., Palladino, M.J., and Wetzel, R. (2018). Mutational analysis implicates the amyloid fibril as the toxic entity in Huntington's disease. Neurobiol. Dis. *120*, 126–138. https://doi.org/10.1016/j.nbd.2018.08.019.

75. Xi, W., Wang, X., Laue, T.M., and Denis, C.L. (2016). Multiple discrete soluble aggregates influence polyglutamine toxicity in a Huntington's disease model system. Sci. Rep. *6*, 34916. https://doi.org/10.1038/srep34916.

76. Ramdzan, Y.M., Trubetskov, M.M., Ormsby, A.R., Newcombe, E.A., Sui, X., Tobin, M.J., Bongiovanni, M.N., Gras, S.L., Dewson, G., Miller, J.M.L., et al. (2017). Huntingtin Inclusions Trigger Cellular Quiescence, Deactivate Apoptosis, and Lead to Delayed Necrosis. Cell Rep. *19*, 919–927. https://doi.org/10.1016/j.celrep.2017.04.029.

77. Leitman, J., Ulrich Hartl, F., and Lederkremer, G.Z. (2013). Soluble forms of polyQ-expanded huntingtin rather than large aggregates cause endoplasmic reticulum stress. Nat. Commun. *4*, 2753. https://doi.org/10.1038/ncomms3753.

78. Hasholt, L., Abell, K., Nørremølle, A., Nellemann, C., Fenger, K., and Sørensen, S.A. (2003). Antisense downregulation of mutant huntingtin in a cell model. J. Gene Med. *5*, 528–538. https://doi.org/10.1002/jgm.378.

79. Evers, M.M., Pepers, B.A., van Deutekom, J.C.T., Mulders, S.A.M., den Dunnen, J.T., Aartsma-Rus, A., van Ommen, G.J.B., and van Roon-Mom, W.M.C. (2011). Targeting several CAG expansion diseases by a single antisense oligonucleotide. PLoS One *6*, e24308. https://doi.org/10.1371/journal.pone.0024308.

80. Zhang, L., Wu, T., Shan, Y., Li, G., Ni, X., Chen, X., Hu, X., Lin, L., Li, Y., Guan, Y., et al. (2021). Therapeutic reversal of Huntington's disease by in vivo self-assembled siRNAs. Brain *144*, 3421–3435. https://doi.org/10.1093/brain/awab354.

81. Dolgin, E. (2022). tRNA therapeutics burst onto startup scene. Nat. Biotechnol. *40*, 283–286. https://doi.org/10.1038/s41587-022-01252-y.

82. Anastassiadis, T., and Köhrer, C. (2023). Ushering in the era of tRNA medicines. J. Biol. Chem. *299*, 105246. https://doi.org/10.1016/j.jbc.2023.105246.

83. Coller, J., and Ignatova, Z. (2024). tRNA therapeutics for genetic diseases. Nat. Rev. Drug Discov. *23*, 108–125. https://doi.org/10.1038/s41573-023-00829-9.

84. Wang, J., Zhang, Y., Mendonca, C.A., Yukselen, O., Muneeruddin, K., Ren, L., Liang, J., Zhou, C., Xie, J., Li, J., et al. (2022). AAV-delivered suppressor tRNA overcomes a nonsense mutation in mice. Nature *604*, 343–348. https://doi.org/10.1038/s41586-022-04533-3.

85. Mendell, J.R., Al-Zaidy, S.A., Lehman, K.J., McColly, M., Lowes, L.P., Alfano, L.N., Reash, N.F., Iammarino, M.A., Church, K.R., Kleyn, A., et al. (2021). Five-Year Extension Results of the Phase 1 START Trial of Onasemnogene Abeparvovec in Spinal Muscular Atrophy. JAMA Neurol. *78*, 834–841. https://doi.org/10.1001/jamaneurol.2021.1272.

86. Buchlis, G., Podsakoff, G.M., Radu, A., Hawk, S.M., Flake, A.W., Mingozzi, F., and High, K.A. (2012). Factor IX expression in skeletal muscle of a severe hemophilia B patient 10 years after AAV-mediated gene transfer. Blood *119*, 3038–3041. https://doi.org/10.1182/blood-2011-09-382317.

87. Sehara, Y., Fujimoto, K.I., Ikeguchi, K., Katakai, Y., Ono, F., Takino, N., Ito, M., Ozawa, K., and Muramatsu, S.I. (2017). Persistent Expression of Dopamine-Synthesizing Enzymes 15 Years After Gene Transfer in a Primate Model of Parkinson's Disease. Hum. Gene Ther. Clin. Dev. *28*, 74–79. https://doi.org/10.1089/humc.2017.010.

88. Mathiesen, S.N., Lock, J.L., Schoderboeck, L., Abraham, W.C., and Hughes, S.M. (2020). CNS Transduction Benefits of AAV-PHP.eB over AAV9 Are Dependent on Administration Route and Mouse Strain. Mol. Ther. Methods Clin. Dev. *19*, 447–458. https://doi.org/10.1016/j.omtm.2020.10.011.

89. Snyder, A., and Grunseich, C. (2021). Hitching a ride on exosomes: a new approach for the delivery of siRNA-mediated therapies. Brain *144*, 3286–3287. https://doi.org/10.1093/brain/awab398.

90. Gomes, A.C., Kordala, A.J., Strack, R., Wang, X., Geslain, R., Delaney, K., Clark, W.C., Keenan, R., and Pan, T. (2016). A dual fluorescent reporter for the investigation of methionine mistranslation in live cells. RNA *22*, 467–476. https://doi.org/10.1261/rna.054163.115.

91. Halfmann, R., and Lindquist, S. (2008). Screening for amyloid aggregation by Semi-Denaturing Detergent-Agarose Gel Electrophoresis. J. Vis. Exp. *17*, 838. https://doi.org/10.3791/838.